Evaluation of Cirrus Cloud Properties Derived From MODIS Radiances Using Cloud Properties Derived From Ground-Based Data Collected at the ARM SGP Site

Gerald G. Mace and Yuying Zhang
University of Utah
Steven Platnick and Michael D. King
NASA Goddard Space Flight Center
Patrick Minnis
NASA Langley Research Center
Ping Yang
Texas A and M

Journal of Applied Meteorology
(Manuscript submitted November 21, 2003)

Abstract: The Moderate Resolution Imaging Spectroradiometer (MODIS) on board the NASA Terra satellite has been collecting global data since March 2000 and on the Aqua satellite since June 2002. Terra has been monitored when it passes close to the ARM sites. In this paper we compare cirrus cloud properties derived from ground-based remote sensing data with similar cloud properties derived from MODIS. In order to improve the space-time correlation between the satellite and ground-based observations, we use data from a wind profiler to define the cloud advective streamline from along which the comparisons are made. In this paper we examine approximately two dozen cases of cirrus and explore a statistical approach to the comparison that relaxes the requirement that clouds occur over the ground-based instruments during the overpass instant. The physical and radiative properties of cloud layers are derived from the MODIS data separately by the MODIS Atmospheres team and the CERES Science Team using multiwavelength reflected solar and emitted thermal radiation measurements. Using two ground-based cloud property retrieval algorithms and the two MODIS algorithms, we show a positive correlation in the effective particle size, the optical thickness, the ice water path, and the cloud top pressure between the various methods although the biases can be significant. Classifying the clouds by optical thickness, we also demonstrate that the regionally averaged cloud properties derived from MODIS are similar to those diagnosed from the ground.

1. Introduction

Cirrus clouds are globally distributed and are composed almost exclusively of nonspherical ice crystals with an annual global and local frequency of occurrence of about 30% (i.e., Wylie et al. 1989; Wylie et al. 1994; Rossow and Schiffer 1999). Satellite imagery shows that large cirrus systems modify the planetary radiation budget by increasing albedo and reducing infrared emission (Liou et al. 1986). Cirrus clouds not only play a significant role in the energy budget of the Earth-atmosphere system by means of their effects on the transfer of radiant energy through the atmosphere, but also are important as a vital link in the hydrological cycle (Stephens et al. 1990, Webster 1994). Given their importance (Lynch et al. 2002), it is necessary to accurately characterize cirrus clouds in models of the global climate (GCMs). However, given the extreme variability of cirrus microphysical properties and the interaction between solar radiation and the nonspherical particles composing cirrus clouds, their role in the climate system is not yet fully understood nor accurately characterized in models.

High level cirrus tend to have low concentrations of large particles relative to most clouds and are, therefore, typically optically thin and gray in the thermal IR spectrum (Ackerman et al. 1988). It has been recognized observationally and through numerical simulation that the influence of optically thin and gray cirrus on the radiation field of the earth-atmosphere system, and hence on weather and climate components of the general circulation, depends on both the solar and thermal IR radiative properties. The radiative properties, in turn, are modulated by the physical composition of the cloud (ice water content, particle size, particle shape and particle concentration) and the physical location of the layer in the atmosphere. In order to place the relevance and importance of cirrus composition, structure and radiative properties into a global perspective and then improve the parameterization of cirrus clouds in GCMs, collections of analysis products including statistical distributions of fundamental cirrus cloud properties are required. Compiling these fundamental data will facilitate investigation of the influence of cirrus clouds on the thermodynamics and dynamics of the atmosphere, and ultimately lead to improved representation of clouds in climate models. Of particular importance in this respect is the need to characterize simultaneously the relationship between the dynamics resolved by a

large scale model, the subgridscale turbulence that ultimately maintains cloud systems and the ice mass and particle sizes that evolve within these environments (Mace et al. 2001).

Present uncertainties in cloud parameterization can be directly linked to the current scarcity of quantitative cloud property observations. In order to build a long term global data set, NASA's EOS (Earth Observing System) project launched its first spacecraft (Terra) on 18 December 1999 (King and Herring 2000). The Moderate Resolution Imaging Spectroradiometer (MODIS; Platnick et al. 2003, King et al. 2003; modis.gsfc.nasa.gov) is uniquely designed with wide spectral range, high spatial and spectral resolution, and near daily global coverage. Upwelling radiation in several narrow spectral channels at a resolution of 1 km in a 2300 km swath under the satellite track is measured by MODIS and converted into cloud properties using various algorithms (King et al. 1992, 1997, 2003; Platnick et al. 2003; Minnis et al. 1995, 1998, 2002). Due to the complex physical processes that relate the retrieved parameters to the upwelling radiances, the error characteristics of the retrievals need to be thoroughly understood before the retrieval results can be used quantitatively to improve our understanding of the role of cirrus in the climate system or to use this knowledge to develop cloud parameterizations for models. The two types of validation approaches expressed in the EOS ATBD (Algorithm Theoretical Basis Document) validation documents are the use of in situ aircraft in short term IOPs (Intensive Operational Periods) and the use of permanent observational facilities to perform validation over a long time period. We use both approaches here.

Given the fine scale variability of most cloud systems including cirrus, there is typically an extreme mismatch between the scales represented by in situ cloud observations collected from aircraft platforms and scales associated with spatially averaged satellite observations. This disparity applies not only to the horizontal dimensions but also to the vertical dimension since the information from solar reflected radiances comprise a non-linear weighting of the cloud properties of individual layers. Since it would take significant time to characterize the volume over which a satellite pixel is relevant, evolution of the cloud system will generally result in temporal changes that will exacerbate the disparity. However, regardless of the problems that are inherent

to the use of aircraft data in satellite cloud property validation, data collected *in situ* remain a valuable source of collaborative measurements and satellite-derived cloud properties should be traceable back to these data sets. In order to effectively use this source of information for MODIS validation, we use a bootstrapping method where the aircraft data are first compared to the results of cloud property retrieval algorithms applied to ground-based measurements (Mace et al. 2002; Dong and Mace 2003) and the ground based results are then compared to those derived from satellites (Zhang 2002). The ground-based remote sensing measurements serve as an intermediate observational scale between the satellite pixel and the in situ observations. Since ground-based retrievals can be more easily validated against aircraft data, our goal is to essentially link satellite retrievals to the *in situ* measurements in this way. This approach has additional benefits. For instance, since ground based instruments can be operated more routinely than can aircraft, we are able to more easily create a statistically significant comparison data set in a shorter period of time.

A proper validation of remotely sensed cloud properties would require enough cloud events to statistically characterize the bias and RMS (Root Mean Square) between the aircraft data and the ground-based data and between the ground-based data and the satellite. This has not yet been accomplished. The necessary aircraft data collected in coincidence with ground-based remote sensors simply does not exist although we use much of what is available as shown in Appendix A. Compiling the necessary number of MODIS coincidences with the ground-based remote sensors simply requires time, and the number of events are growing. In this paper, our goal is to illustrate our methodological approach to building a reasonable space-time correlated comparison between the ground-based results and cloud properties derived from MODIS data, and to present a preliminary comparison of a number of thin cirrus events. We also demonstrate a statistical approach to validation that measures whether relationships between certain cloud properties are similar between the ground-based and space-based retrievals. In any comparison of cirrus cloud particle sizes, a careful accounting must be made of the differences in the definitions of particle size. Appendix B explores this issue for the algorithms used here.

2. Comparison Technique

We use two ground-based retrieval algorithms to compare with satellite-derived cirrus cloud properties. In this section we illustrate the use of an algorithm that relies on radar reflectivity and Doppler velocity (hereafter referred to as the Z-velocity algorithm; Mace et al. 2002; Mace 2003). The technique is applied to the ground-based data collected by the MMCR (Millimeter Cloud Radar; Moran et al. 1998) at the ARM sites. Concentrating on the capacity of the moments of the Doppler spectrum to provide information suitable for retrieving the microphysical properties of cirrus clouds, this algorithm uses the zeroth and first moments of the Doppler spectrum (radar reflectivity and mean Doppler velocity) to retrieve the cloud particle size distribution. This technique uses only measurements from the MMCR to retrieve the cloud properties, so it provides certain practical advantages compared to those requiring multiple instruments. An advantage of this technique over the Z-Radiance approach described in Appendix A and used in the next section, is that the Z-Velocity algorithm has much higher (36 s) temporal resolution and provides vertically resolved cloud properties. It also can be applied without requiring the layer to be optically thin and observable without the presence of lower level clouds. However, the approach cannot be generally used since in only a limited number of situations can the vertical air motions can be reliably separated from the particle motions (Mace et al. 2002).

Since the satellite observations represent a single moment in time over an area and the ARM data provide a time series from a single location, we apply a simple technique to improve the space-time correlation between the observations. Using data from the Lamont 404 MHz NOAA wind profiler (36.6N 97.5W) that is 11 km from the SGP site, we define a streamline along which the observed cloud has passed in the 30 minute period both before and after the satellite overpass. Data are extracted from the MODIS-derived cloud products on either side of a 30 km wide streamline to create statistics of the cloud properties that would pass near the SGP site. While the approach has obvious advantages, an assumption of stationarity in the cloud field properties during the 30 minute advection period does not always hold and features that exist in the 30 km swath do not always pass over the cloud radar. However, this approach does lead to more

robust comparisons in many cases. For example, MODIS passed over the ARM SGP site at 17:35:57 UTC with a view zenith angle of 1.3° on 6 March, 2001 (Figure 1). Figure 2 shows the wind profile at Lamont on 6 March, 2001. After tracking upstream and downstream 45 km from the ARM site to represent approximately 1 hour of ground data centered on the overpass, there are 7062 MOD06 pixels to compare with the ground-based observations. The operational pixel-level MODIS cloud product is archived under the file designation MOD06 (Platnick et al. 2003; King et al. 2003), and will be referred to as such throughout this paper. This product chooses the default cloud particle effective radius to be the one retrieved using the 2.1 μm MODIS band (though information for separate retrievals using the 1.6 and 3.7μm bands are also available). The MOD06 data used in the comparisons are collection 4. The frequency distributions of selected cloud properties from MOD06 and those from the corresponding MMCR retrieval are displayed in Figure 3.

The cloud particle size compared here and in the remainder of the paper is the effective radius as defined by the MOD06 retrieval algorithm to be proportional to the ratio of the volume of ice to the projected area (specifically re=3/4*V/A) of the particle size spectrum where the geometric quantities are derived from a combination of various particle habits that vary with effective radius (Platnick et al. 2003). The forward radiative transfer computation involved in the MOD06 retrieval algorithm assumes plates, hollow columns, bullet rosettes, and aggregates with habit percentages derived from the statistics of a number of field campaigns. The detailed information regarding the information on particle habits and size distributions used in MOD06 can be found in King et al. (2003). The relationships between the particle size definitions used in this paper are discussed in Appendix B. We find in this case that the effective sizes agree well between the MOD06 and Z-Velocity algorithms with the mean values near 30 μm and 28 μm respectively. The standard deviation of the MOD06 sizes is larger than derived from the ground although this is expected given the wider geographical domain evaluated compared to the effective domain examined by the ground-based data. The MOD06 IWP also has a wider spectrum ranging from $5\,g/m^2$ to $120\,g/m^2$ and a lower modal IWP of about $53\,g/m^2$, while the ground-based retrieval has a narrower spectrum ranging from $30\,g/m^2$ to $90\,g/m^2$ and a bi-modal frequency distribution with one mode similar to the MOD06

result and the other somewhat higher at about $62\,g/m^2$. Both satellite and surface retrieved optical thickness vary from 1 to about 5, while the mode value from MOD06 is 2.5 and that from surface measurement is around 3.4. However, the mean optical thickness for both methods is similar at around 2.4 with a standard deviation of 0.34 and 0.68 for the ground-based and MOD06 results, respectively.

Figure 4 shows a similar comparison of cloud optical properties retrieved using MODIS data by the CERES science team (Minnis et al. 1995, 1998, 2002). These pixel-level retrievals are used internally by the CERES team, though statistics over the CERES sensor footprint are archived along with other CERES data. The default cloud particle effective radius is derived from the 3.7 μm MODIS band (as opposed to default use of the 2.1 μm band by MOD06). With the exception of the particle size, the MODIS-CERES results are in somewhat better agreement with the ground-based retrievals in terms of the mean, mode and standard deviation. The MODIS-CERES particle size tends be larger on average (~32 μm) and spread over a wider range. The comparison between these two retrievals from the MODIS observations is given in Figure 5 and all the comparisons are summarized in Table 1.

Since certain assumptions have been made in the formulation of the ground-based retrieval algorithm, there is some inherent error in the statistics. Using a realistic comparison to aircraft in situ data, the algorithm uncertainty is found to be on the order of 60% in IWC and 40% in mean particle size (Mace et al. 2002). However, the precision of the results seems to vary substantially from case to case due primarily to the ability of the processing methodology to accurately separate air motions from the particle motions in the Doppler velocity. This error introduces a difficult to quantify case-dependent bias in the results. Other algorithm assumptions also contribute to the error. For instance, we assume that the cirrus particle size spectrum can be approximated by a simple unimodal exponential distribution. While bimodal size distributions are a frequent occurrence at warmer than average cirrus temperatures and at larger than average radar reflectivities for cirrus, Mace et al. (2002) found using aircraft data that significant error is first encountered at radar reflectivites more than about -5 dBZe. Radar reflectivities of this magnitude and greater are found in the middle of the cirrus layer beginning from 17:15:00 UTC (Figure 1a) and contribute to the IWP mode found near $60\,g/m^2$, but the

mean value expresses the cloud properties more reliably because of the insignificant difference between the two modes. The mean IWP of the MOD06 cloud product is somewhat higher than the mean IWP of ground-based results. The comparisons suggest that the three retrieval algorithms interpreted the cloud field on this day in a similar manner. However, we do find substantial biases between the MOD06 retrievals of cloud top pressure and temperature compared to the ground-based observations (Figure 6). The satellite-derived values appear to be substantially larger than observed with the radar.

3. Comparison of thin cirrus

While the Z-Velocity algorithm shows considerable promise as a tool for cloud property validation, this algorithm is still undergoing development and testing and has not yet been extensively applied to the ARM data. Another algorithm (hereafter referred to as the Z-radiance algorithm) based on combining the layer-mean radar reflectivity and the downwelling radiance observed by the Atmospheric Emittance Radiance Interferometer (AERI; Smith et al. 1998) has been updated and thoroughly tested using available in situ data and applied to the entire ARM SGP MMCR data stream. This algorithm is especially designed to derive the microphysical properties of optically thin cirrus layers with infrared emissivity less than approximately 0.85 that occur with no lower cloud layers. A description of the updated algorithm, a sensitivity analysis, and in situ validation are included in Appendix A. We show that based on comparison to in situ data, both the IWP and the layer-mean effective radius can be derived to within 20%. Since the Z-Radiance algorithm has reasonably understood error characteristics, we are able to address the comparison of the ground-based cirrus retrieval to cloud properties derived from coincident MODIS data.

Traditionally, the approach to validation is to gather events that lend themselves to comparison of one result against another. When enough events have been compiled to form a statistically significant set of comparisons, some estimate of the goodness or lack thereof can be ascertained. While this approach is reasonable, it can take considerable time to gather a set of narrowly defined cloud events that occur when all the necessary ground-based instruments are operating and the satellite passes overhead and observes the same cloud. For instance, it make no sense to attempt to compare cloud properties in

situations where the satellite algorithms attempted retrievals in only a small subset of apparently cloudy pixels observed during the 1 hour period surrounding the overpass. Consider the data collected on March 22 2001. Figure 7 shows the MMCR data collected during the overpass period while the cloud properties retrieved from the Z-Radiance algorithm are shown in Figure 8. Figure 9 shows the 1.38 μm channel MODIS imagery and the associated MOD06 retrieved optical thickness. The 1.38 μm channel is particularly sensitive to observations of thin cirrus because water vapor concentrated in the lower troposphere absorbs strongly in this channel highlighting cirrus reflectance in the upper troposphere (Gao et al. 1993, 1995). In this case, the viewing zenith angle is 2.5°. The thin cirrus is overcast during the 3 hours around the overpass time according to the MMCR, but when we track along the wind direction (285°) with speed 30m/s, there are only 688 points from the 2768 MODIS pixels that have identified cirrus occurrence. The time series of ground-based retrievals show that the cirrus becomes quite thin with optical thickness less than 0.5 during the period surrounding the overpass. From the frequency distribution of the MOD06 optical thickness displayed in Figure 10, there is no optical thickness retrieved less than 1. The derived cloud-top pressure (Figure 11) is also much higher for this event than the radar-observed cloud top pressure. The cases we present below have, therefore, been screened so that events with significant biases in terms of detection like on March 22 are excluded. Of course, the cases have not been screened to find only the best comparisons in terms of cloud properties although, as we demonstrate, this problem does influence the comparison results in many cases.

3.1 Comparison of individual cases

Table 2 lists 15 Terra overpasses of the SGP ARM site that have cirrus of the proper type (optically thin and single layer) existing concurrently with all necessary ground-based data, and Figure 12 shows the comparison of the Z-Radiance and MOD06 cirrus properties. In these comparisons, the satellite-derived mean and standard deviation are compiled using the technique outlined in the previous section while 1 hour of Z-Radiance data are used to form the mean value shown in the plot. The error bars attributed to the ground based results are the fractional uncertainties that we derived from the aircraft data comparison shown in Appendix A. There are 9 cases of the 15 for which the MODIS-CERES retrieval results are also available (Figure 13). A summary of the

comparison is in Table 3 where we show the linear correlation coefficient, the slope of a best fit linear regression, the bias, and the bias standard deviation.

Clearly, these comparisons suffer from an insufficient number of events although useful information if not generalities can be inferred from the comparisons. One must take care not to infer too much from the statistics in Table 3, however. We do find some degree of linear correspondence in all the comparisons with a positive linear fit although the optical thickness, and r_e in the MOD06 are only weakly correlated as expected when the thin cirrus is excluded. The bias in the MOD06-derived IWP, r_e and optical thickness are positive and it seems by inspecting Figure 12, that the positive bias tendency is more pronounced for the more tenuous clouds. This characteristic is most obvious in the optical thickness comparison. Whereas several of the ground-based results have event-mean values significantly less than 1, the MOD06 mean values never decrease to less than 1.

Overall, the comparison between the ground-based results and the MODIS-CERES retrievals are somewhat better than found with the MOD06 results. For all three parameters, the correlation tends to be higher, the slope of the linear regression line is closer to 1 and the biases tend to be smaller. Visually, the optical thickness scatter plot seems to be more closely aligned with the ground based quantities than is found with the MOD06. Note that several of the cases with optical thickness less than 1 correlate well between the Z-Radiance and the MODIS-CERES results.

The disagreement between the satellite and ground-based cloud properties may arise from several sources of uncertainties associated with the satellite and ground-based retrieval algorithms. For instance, one of the reasons for the disagreement between the satellite and ground-based retrieval may be the vertical inhomogeneity of clouds. For midlatitute cirrus clouds, it has been observed that ice crystals in the top layers are normally small pristine particles with well-defined hexagonal structures whereas ice crystals in the bottom layers are large irregular particles. The effect of this inhomogeneity is small for visible channels, but it can be quite significant for near-IR and IR channels for which ice are strongly absorptive. The directional scattering characteristics of cirrus are known to be a function of the cloud particle habits. In order to compile the 15 cases included here, we used view zenith angles that range from very small to very large and

covered a range of solar zenith angles. Ideally, we would like to characterize the errors as a function of relative zenith, but this will require additional time to build up the case study data set. Also, since we are concerned primarily with optically thin clouds, any error in the assumed surface albedo will have a detrimental effect on the satellite-derived results. For example, a cirrus cloud with an optical thickness of 0.5 over a black surface might be expected to have a bidirectional reflectance in the range 3-4% for a visible band and typical solar/viewing geometries. Spectral surface albedo maps used by MOD06 (Platnick et al., 2003) for the MODIS 0.65 μm band vary from about 8-13% for crop mosaic and grassland ecosystems, a range as large as the cirrus reflectance itself. However, even though the number of cases is small making the comparison quite preliminary, intriguing aspects can still be deciphered from the comparisons. For instance, it appears that there is a tendency for the error bias in the spatially averaged MOD06 results to increase for increasingly thin cirrus fields while this tendency is not seen in the MODIS-CERES results. This behavior may be due to the fact that the cloud identification scheme in the MOD06 product is being applied conservatively over this ecosystem as previously discussed and some cloudy pixels are not being processed. This would tend to cause the area-averaged cloud properties to be biased high and would tend to cause the bias to increase as the cloud fields in question become more tenuous on average. The MODIS-CERES cloud identification scheme does not appear to suffer from this problem.

In order to examine the validity of the cloud top retrievals, the cloud top heights are compared between the surface data and the satellite data. We convert the cloud top pressure and temperature found in the MOD06 files to cloud top height using thermodynamic profiles collected at the ARM site. Based on the comparisons in Figure 14 and Table 3, we find that the satellite-derived cloud top heights are generally lower than those detected by the ground-based cloud radar. This bias appears to be more pronounced in the MODIS-CERES retrievals (Figure 14b) than in the MOD06 results (Figure 14a).

3.2 Statistical Comparison

It is a challenge to acquire a statistically significant set of events when cirrus, satellite, and ground-based instrumentation all exist at a particular location simultaneously. Because of this, we would like to explore an approach that allows us to examine the similarity of certain relationships within the ground-based and satellite-derived descriptions of cirrus. This approach assumes that, in the region surrounding the ARM site, the properties of a given class of cirrus are similar to the same class of cirrus observed at the ground site. In essence, this assumption allows us to compile statistical distributions of some quantity from cirrus clouds observed at the ground site during periods when clouds are present but MODIS is not and compare these distributions to similar distributions compiled from MODIS retrievals of cirrus that do not necessarily occur at the ground site but within the region surrounding it. We have collected the overpasses of 648 events from March 2000 to July 2001 when Terra passed near the SGP site in the daytime and identify cirrus within a 100 km x 100 km area centered on the SGP site. The cirrus reflectance and the cloud top pressure in the MOD06 file are used to identify the occurrence of cirrus. When the cloud reflectance is positive, the cloud top pressure of a pixel is less than 500hPa, and the optical thickness is less than 5, this pixel is counted in the statistics as cirrus. We consider 895,243 MOD06 high cloud retrievals in the 100 x 100 km region.

We compare the composite properties of MOD06 thin cirrus observed in the SGP region with similar properties derived from a record of cirrus observed by the MMCR at the SGP site. We have identified the cirrus events at the SGP site with the Z-Radiance algorithm for the same time period in terms of years and months as the MODIS data, amounting to a total of 5772 3-minute averages or approximately 300 hours of cirrus. The occurrence distribution of the MODIS pixels and the SGP points categorized by optical thickness are depicted in Table 4. Clearly, the MODIS and ground-based distributions are weighted much differently with respect to optical thickness. For the ground-based data the thinnest optical thickness bin contains more than a factor of 3 more events than the 0.5-1 optical thickness bin with the number of occurrences decreasing exponentially toward high optical thickness. Similar distributions of cirrus optical thickness have been reported in other mid latitude data sets (Mace et al. 2001, Comstock and Sassen 2003; and Comstock et al. 2002). The MOD06 frequency, on the other hand, peaks in the 1.0-

1.5 optical thickness bin with more than an order of magnitude fewer pixels in the 0.5-1.0 optical thickness class. This behavior lends some credence to the idea that the bias identified in Figure 12 arises from the MOD06 algorithm not processing thin cirrus pixels over this region.

The frequency distributions of MOD06 and Z-Radiance r_e and IWP within several visible optical thickness ranges are shown and compared in Figures 15-18. It is interesting to note that the effective radius distributions for the various optical thickness ranges do not change a great deal from the thinnest to thickest optical thickness considered here. There is some tendency for the mean particle size to increase from the thinnest to thickest optical thickness, but the distributions tend to remain broad. The IWP does tend to shift noticeably from a narrow nearly exponential distribution shape to a more normal but broad distribution for the higher optical thickness classes. This evolution in IWP is more noticeable for the Z-Radiance statistics. This leads to a noticeable bias between the Z-Radiance and MOD06 histogram in the highest optical thickness class considered. Overall, however, the agreement between the MOD06 and ground-based cloud properties is reasonable. Both algorithms show the clear trend toward higher values of IWP and larger particle sizes as the optical thicknesses increase.

4. Summary

In order to improve our understanding of the role clouds play in the climate system, global cloud property retrievals are being conducted using the data sets being created by MODIS on the Terra and Aqua satellites. The retrieval algorithms that are implemented by the MODIS atmospheres team (MOD06; Platnick et al. 2003) and by the CERES science team (MODIS-CERES; Minnis et al. 1995) use reflected visible and near infrared radiances to infer the optical thickness and effective particle size of underlying clouds. While, several recent studies have examined the validity of water cloud properties derived from the MODIS sensor (Dong et al. 2003), the error characteristics of these data sets for other cloud types including cirrus are largely unknown. In order for these global cloud products to be utilized for their intended purposes, validation continues to be necessary. Using data collected at the ARM SGP site, we have made a

first attempt at using ground-based data to systematically validate cirrus cloud property retrievals from the MODIS algorithms.

The approach we have taken attempts to transfer the standard supplied by aircraft data to events observed by the satellite imagers as they passed over the ARM site using the ground-based algorithm results as an intermediate step. This approach requires a thorough validation of the ground-based algorithms with aircraft data and development of an extensive set of satellite-ground based events. While neither of these requirements has been satisfied to a level where statistical significance can be unambiguously established, we decided to present the data here in a preliminary form to illustrate the general approach and to consider some early generalizations of our findings so that improvements can be pursued while the data sets continue to grow.

Several issues were addressed that make comparison of passive satellite imager retrieval results with ground-based data a challenging exercise. These range from issues associated with establishing the validity of the ground-based retrievals (Appendix A) to accounting for differences in the definitions of effective particle size between the various algorithms (Appendix B). Also, since clouds pass over the narrow field of view and vertically pointing ground-based instruments as they are advected along the wind, some technique beyond simple spatial averaging of a heterogeneous cloud field must be considered in order to conduct reasonable comparisons. This preliminary step in the comparison process is especially important in cirrus clouds since cirrus tend to exist in fast moving airstreams and have significant heterogeneity across the flow. Using wind profiler-observed horizontal wind direction and speed and knowledge of the cloud location in the vertical column, we were able to construct a rectangular box within the imagery whose long axis was oriented along the wind direction with a length proportional to 1 hour of advection time. This rectangular region was centered on the ground site and had a cross stream length of 30 km. We found that comparisons of the MODIS retrievals averaged over a region defined in this way to 1 hour of ground-based data centered on the overpass time provided superior results compared to simple regional averages that did not consider the advective streamline.

A set of 15 individual events were compiled from several years of Terra MODIS overpasses of the ARM SGP site during which single layer optically thin cirrus were

observed by the MMCR. The Z-Radiance algorithm (Appendix A) was applied to this data and the comparisons presented in Figures 12 and 13. We found that a high degree of linear correlation exists in the comparison set considered here. In general the MODIS-CERES results showed better overall agreement compared to the ground-based data. The source of disparity in the spatially-averaged MOD06 results occurred preferentially when the optical thickness of the cirrus retrieved from the radar data was less than about 1.0. As discussed, MOD06 takes a more conservative approach to the detection of thin cirrus before a retrieval is attempted. While this apparently biases the thin cirrus comparisons, what has not been studied is the occurrence of false positives in these satellite algorithms, i.e., cases where retrievals are attempted but cirrus is not detected from the ground or not thick enough to allow for reliable retrievals from solar methods. In several cases, the optical thickness derived from the ground-based data decrease to values approaching 0.5 while the area averaged MOD06 optical thickness remained at or above 1.0. In layers that were more optically thick, both algorithms appeared to perform equally well when compared to each other (Figure 5) and to the ground-based results (Figure 3, 12, 13). These findings have clear implications for the spatially averaged Level-3 products being created with MOD06 retrievals (MOD08_D3) and suggest that cirrus cloud properties over continents may be biased toward the less frequent optically thicker cirrus clouds.

Reasoning that the properties of clouds observed in a region surrounding the ARM site by MODIS should be similar to the properties of the clouds observed at the ARM site by the ground-based instruments, we relaxed the requirement that the clouds be observed simultaneously by both instruments and examined the frequency distributions of IWP and re for different optical thickness classes. Comparing high cloud occurrence in a 10^4 km^2 region centered on the SGP site from 648 overpasses with cirrus cloud properties derived from ground based data collected during the same period of time (March 2000-July 2001), we found that the frequency distribution of optical thickness for high clouds in the MOD06 product were very different from that observed at the ARM site (Table 3) with relatively few occurrences of cirrus with optical thickness less than 1.0 as compared to the ground-based data where the optically thinnest clouds were the most frequently observed. Comparing the derived microphysical properties in various optical thickness classes, we found that the frequency distributions of IWP and effective radius agree

reasonably well. An IWP bias is apparent in the optical thickness 3-5 category. However, relatively few observations were available from the ground-based data in this category.

Overall, with the exception of cloud top height, we find that the cirrus cloud properties reported in the MOD06 and MODIS-CERES retrievals agree reasonably well with the aircraft-validated ground-based cirrus cloud properties. The tops of cirrus layers diagnosed from the MODIS algorithms are biased low by at least several hundred meters on average with the bias appearing to increase with optically thinner clouds. We find that the MOD06 significantly underreports the occurrence of cirrus with optical thickness less than about 1.0. We infer this from case studies (Figures 7-11) and long-term statistics of cloud properties (Table 3). This tendency results in the characteristic observed in Figure 12 where the optical thickness of thin clouds are biased high. The MODIS-CERES results do not show this tendency and thus have better overall agreement (Table 3).

This work is preliminary in the sense that many more cases are needed to establish a high degree of statistical significance so that numerical values can be applied to the uncertainties in the retrieved cloud properties. So long as the ground-based instruments operated by the ARM program continue to be operational, only time is needed to generate additional coincident cases. Our eventual goal is to investigate the error characteristics in the MODIS-derived cloud properties as a function of the viewing geometry of the instrument and as a function of ecosystem. For instance, do we find similar errors in thin cirrus reporting over the tropical oceans or over the polar regions? Since we have only examined cases observed by MODIS on the Terra satellite, do we find similar issues with the MODIS instrument on Aqua? Also, since the MODIS cloud mask algorithm varies with ecosystem type, each ecosystem should be considered separately. Furthermore, the reflected radiance observed above optically thin clouds are sensitive to the surface albedo. We would expect to find some sensitivity to errors in surface albedo in the reported cloud properties.

In terms of improving our confidence in the ground-based retrievals, additional aircraft data are clearly needed to establish more rigorous uncertainties in the ground-based algorithm results. Since statistical significance in validation will not be accomplished without an increase in the number of direct aircraft-ground site comparisons, it seems clear that if the atmospheric research community places value on

rigorously characterizing the uncertainties in global cloud property retrievals, then an investment in the quantity of aircraft-ground site comparisons should be made a high priority.

Acknowledgements: This research would not have been possible without substantial assistance from several individuals on the MODIS Atmospheres and CERES science teams including Dr. William Ridgway who provided access to MODIS data and products. Mr. Michael Poellot and the University of North Dakota Citation team worked hard during several field campaigns at the ARM SGP site. Data were obtained from the Atmospheric Radiation Measurement Program sponsored by the U. S. Department of Energy, Office of Science, Office of Biological and Environmental Research, Environmental Science Division. Specifically, we would like to thank Mr. Jim Teske and staff at the SGP site for keeping the instruments functioning and the data flowing in a sometimes challenging environment. Funding for this work was provided by a NASA EOS Validation Program grant (NAG56458), by the Environmental Science Division of the U. S. Department of Energy (Grant DE-FG0398ER62571).

Appendix A: The Z-Radiance Algorithm

The Z-Radiance algorithm (Mace et al. 1998; Zhang 2002) retrieves the layer-mean properties of optically thin cirrus by combining observations from the MMCR and Atmospheric Emitted Radiance Interferometer (AERI) at the ARM sites. One of our primary assumptions is that the layer-mean particle size distribution (PSD) can be approximated by a modified gamma function (Gossard, 1994; Dowling and Radke, 1990). Expressing this function in terms of the modal diameter the distribution function can be written,

$$N(D) = N_x \exp(\alpha)\left(\frac{D}{D_x}\right)^{\alpha} \exp\left(-\frac{D\alpha}{D_x}\right) \qquad (A.1)$$

where Dx is the modal diameter and Nx is the number of particles per unit volume per unit length at the functional maximum.

Assuming that the particles are small compared to the wavelength we can use the Rayleigh scattering approximation and write

$$Z = N_x e^{\alpha} D_x^{7} \frac{(6+\alpha)!}{\alpha^{7+\alpha}} \tag{A.2}$$

The IWC and r_e, based on their definitions, can also be expressed as a function of D_x and N_x. The two unknown parameters, N_x and D_x, of the modified gamma distribution can be determined from the observed downwelling radiance and the radar reflectivity using an expression for the cloud layer emittance ε

$$\varepsilon = 1 - \exp[-(1-\overline{\omega_0})\bar{\beta}\Delta h] \tag{A.3}$$

by relating the extinction coefficient and single scattering albedo to the distribution parameters using the radiative parameterization described in Fu (1996) or Fu et al. (1998) and the definition of the effective radius and IWC.

Through an iterative scheme, a layer mean size distribution is found that simultaneously returns the observed radar reflectivity and the downwelling radiance as observed by the AERI when the radiative properties of the particle distribution are inserted into the MODTRAN3 radiance algorithm (Berk et al., 1989).

To estimate the sensitivity of the Z-Radiance algorithm to uncertainties in the input data, we use a fractional deviation which is defined as

$$\delta_{IWC,re}^{2\sigma} = \frac{C_{sta} - C_{dev}}{C_{sta}}$$

where C_{sta} is the IWC or r_e value calculated using an unperturbed radar reflectivity factor and an unperturbed layer emittance, C_{dev} is the IWC or r_e value calculated using a perturbed radar reflectivity or a perturbed layer emittance.

In the sensitivity analysis of the Z-Radiance algorithm, a representative range in radar reflectivity from –6 to –40 dBZe is used and the cirrus emittance is varied from 0.1 to 0.9. The layer thickness is set to 1 km. Because the calibration error for the MMCR is about 1 dBZ, the deviation from the representative values is assumed to be multiples of 1 dBZ. And because the AERI radiance error is relatively small, we use multiples of 0.01 (less than about 10% of representative values for cirrus emittance) as the deviation. The

changes of r_e and IWC with the error of observations and the standard deviations are calculated. The results for the perturbed analysis of IWC and r_e are shown in Figure A.1 and Figure A.2, respectively. We find that calibration errors up to 5 dBZ in the radar lead to errors as large as 50% in the IWC and 22% in the effective radius with an inversely proportional relationship between the calibration errors and the retrieved values. Errors in the AERI radiance up to 5% result in IWC errors of 13% and errors in the effective radius of just -4%.

It is important to establish the validity of the ground-based retrievals with independent observations also. Since in situ measurements can provide reliable information about actual cloud properties, microphysical data collected in cirrus clouds by aircraft can help build a better understanding of the validity of the algorithm. The University of North Dakota (UND) Cessna Citation II aircraft, operated by the Department of Atmospheric Sciences at the UND for various research projects, is equipped with several instruments used to collect meteorological data and has been used in research projects for the ARM Program. We use here the record of cirrus in situ data that has been collected at the SGP CART site during IOPs between 1997 and 2000 (Poellot et al., 1999) with Particle Measuring Systems (PMS) probes (Heymsfield and Parrish, 1986).

The basic measurement consists of the 5-second averaged particle size spectrum recorded by the 2DC. From this we calculate the ice water content and effective radius. It has been shown that the bulk density of cirrus particles decreases with an increase of their dimension D as inferred from 2D particle images (Brown and Francis, 1995). It is also well known that the shapes of cirrus crystals have high variability (Weickmann, 1948; Liou, 1986), and change with temperature and cloud type (Heymsfield and Platt, 1984). This characteristic of cirrus results in substantial difficulty when attempting to derive water content from measured particle spectra. There have been many schemes for parameterizing the masses (M) of ice particles to determine the ice water content. In this study, a simple and direct method proposed by Mitchell (1996) is used in the form of mass-dimensional power-law expressions:

$$M = \alpha D^{\beta}$$

where D is maximum dimension measured by the 2DC, and different coefficients are used for various ice particle types. The coefficients we use are copied from Mitchell

(1996) and are listed in Table A.1 and shown Figure A.3. These Particle habits correspond to the typical range of particle habits observed in midlatitude cirrus clouds. The masses of ice crystals vary substantially when calculated with different coefficients. Therefore, for every size distribution spectrum, we calculate the ice crystal mass for every kind of crystal shape listed in Table A.1 and then consider the mean and standard deviation of the various habits to allow for a reasonably estimated range of uncertainty of the IWC sampled by the aircraft.

The clouds were sampled by the UND Citation with a flight strategy that was designed to generate an unbiased statistical sample of the cirrus layer properties as they advected over the ground-based instrument suite: 1. the aircraft started either near cloud base or top and stepped up or down at approximately 300m increments after performing a level leg of approximately 20km centered on the SGP ground site; 2. the cloud layer was profiled in this way and then a spiral of approximately 5km radius was conducted centered on the SGP site through the layer; 3. the pattern was repeated as long as the cloud and aircraft fuel permitted. Depending on the flight profile (level legs or spiral) we use two approaches to calculate the ice water path from in situ measurements: first, for a series of stepped level legs that profile the cloud layer, the leg-averaged value of IWC are considered valid over a vertical depth that is taken to equal the aircraft altitude change between legs. The vertical integral is approximated as the sum of these legs; second, for the spiral profile, a more robust integral is approximated by summing the IWC over the vertical depth applicable to each 5-second interval.

A comparison of 13 individual cases between the layer-mean retrieved cloud properties and similar properties derived from aircraft profiles of cirrus using data collected during cloud IOPs at the SGP site is shown in Figure A.4. Because the 2DC is most reliable in the particle range between approximately 100 and 700 microns, we compare the IWC and effective radius only in that size range; the observed and retrieved size distributions are integrated from 100 μm to 700 μm. As can be seen in Figure A.4, we find a high degree of linear correspondence between the observations and the retrievals. The linear correlation coefficient is 0.92 for IWP comparison and 0.91 for the r_e comparison with an RMS for both r_e and IWP between 20% and 25% of the mean

values. The mean bias is 2.676 and -1.846 for r_e and IWP, and the bias standard deviation is 10.79 and 10.86 for r_e and IWP, respectively.

To build further confidence in the retrieval results, the solar radiative effects derived from layer-averaged cirrus properties are examined. Since the cirrus-layer properties derived from the retrieval algorithm will produce the correct downwelling radiation in the infrared portion of the spectrum, we compare, when possible, the downwelling solar flux observed at the surface with calculations of the solar flux that use the derived microphysical properties.

The observed fluxes are expressed in terms of the fraction of the clear sky flux at the surface removed by the cloud layer, that is, the solar forcing which is employed in many radiative field studies (Shi, 1994; Mace98; Mace et al., 2001). The observed clear-sky fluxes are determined following Long (1996).

The normalized cloud forcing (Cf) is defined as

$$C_f = (F_{clear} - F_{cloud}) / F_{clear}$$

where F_{cloud} is the observed downward surface shortwave flux in the presence of clouds; and F_{clear} is the clear-sky value calculated from the radiative parameterization.

The solar forcing calculated from the retrieved cloud properties from July 2000 to July 2001 at the ARM SGP site are used here. The mean of the calculated forcing values is binned in 0.015 forcing increments, and the standard deviation is calculated. The comparison is shown in Figure A.5: (a) is the comparison between the observations and the Mace et al. 1998's algorithm results which use Fu and Liou 1993's parameterizations and (b) is the comparison between the observations and the updated Z-Radiance algorithm results using Fu's improved radiative parameterizations (Fu 1996, Fu et al. 1998). For the correlation coefficient for both comparisons, (a) is 0.834 while (b) is 0.886. The RMS (root mean square) for both re and IWP are between 20% and 25% of the mean values. The improvement in the updated results can be seen more obviously from 0.15 to 0.35 interval of the cloud forcing value. The linear relation is stronger for the updated algorithm. For small values of cloud forcing, the difference is caused by limitations in the radar measurement. When cirrus clouds are thin, the radar cannot detect the full depth, so the layer mean Z_e is likely biased high and the resultant calculated forcing values are biased high as in Figure A.5 for C_f smaller than 0.1. Our algorithm is not applicable to

thick cirrus ($\varepsilon \geq 0.9$), so the cloud forcing comparison is limited to values smaller than 0.4. This equates to visible optical thickness about 4.

Appendix B. Cirrus cloud particle size comparison

One of the more challenging aspects of comparing the retrieved properties of ice clouds is accounting for the different definitions of particle size. There have been several studies that have attempted to make some sense of this subject (e.g. Mitchell, 2002). While it is not our goal to review that work here, it is important to understand the difference between the definitions of particle size that are used in the ground-based remote sensing algorithm, that used in our comparison of the ground-based data to aircraft data in appendix A and the definition of particle size used in the algorithms applied to MODIS data. Understanding these definitions and the relationships between them are necessary because often a single number is used to characterize a size spectrum that, in a sample volume, can have particle sizes ranging from a few 10's of microns to perhaps a millimeter or larger. Since the observational methodology ranges from direct measurement by in situ instruments to probing cloud layers with visible light and microwaves, the observations themselves are naturally weighted to different moments of the size spectrum. The typical aircraft probes used in cirrus research (the PMS 2DC, for instance), are often not sensitive to small cirrus particles (less than 100 microns) and do not have sample volume sufficient to accurately characterize particle numbers in the millimeter range and larger. Satellite remote sensing often relies on probing the cloud layers with light in the visible and near infrared portions of the spectrum where the 2^{nd} moment of the particle size distribution (the cross sectional area) contributes heavily to the measurement. Millimeter radar, on the other hand, derives its signal from the higher moments of the size distribution (i.e. the sixth moment if the particles are solid and small with respect to the wavelength) and is, thereby, weighted to the largest particles. The retrieval algorithms, evaluated in this paper, are essentially designed to convert from the moments of the distribution measured by the instruments to other moments of interest. For instance, the radar retrievals described earlier attempt to convert the measured sixth moment into a general description of the size distribution from which any other weighted

quantities can be derived. Our goal is to evaluate the relative success of these conversions through comparison. However, we must first understand the definitions of the different particle size descriptions used in the algorithms and the relationships between them.

Since aircraft make the most direct measure of the particle size distribution and aircraft measurements are most closely in tune with the nonsphericity of the particles, the maximum dimension or some variant of it (Brown and Francis, 1995) is typically used to describe the sizes of the particles. Use of the maximum dimension as the characteristic ice particle dimension has resulted in a number of authors attempting to quantify the amount of condensed water and projected ice surface area within the volume of a sphere circumscribed around the maximum dimension (e. g. Heymsfield and Platt, 1984; Mitchell 1996, Heymsfield et al., 2002). Such papers often discuss an effective ice crystal density (ρ_{eff}) that decreases from that of solid ice for small spheroidal particles to values that are quite low (~0.1 g/cm3) for millimeter size nonspherical particles (Brown and Francis, 1995). These relationships tend to be strongly habit dependent as shown by Heymsfield et al. (2002) and others. In order to facilitate comparison between aircraft data and cloud properties retrieved from ground based radar data, we have derived the ground-based retrieval algorithms in terms of particles sizes related directly to the maximum dimension. This approach has necessitated specification of some relationship between the size and effective density. In the Z-Radiance algorithm, we use the description of effective density found by Brown and Francis (1995) while in the later Z-Velocity algorithm, we use a temperature dependent combination of the mass and area-dimensional relationships reported by Mitchell (1996).

Retrieval algorithms that use optical measurements typically retrieve the effective radius (r_e) which is defined by Hansen and Travis (1974) for spherical particles as the ratio of the third moment of the size distribution to the second moment of the size distribution or $r_e = \frac{\int a^3 n(a)\,da}{\int a^2 n(a)\,da} = \frac{\langle a^3 \rangle}{\langle a^2 \rangle}$ where a is particle radius and the angle brackets denote an integration over the size spectrum to derive a moment. It can be shown easily that in the case of particles that are large with respect to the wavelength of light (i.e., the case when extinction efficiency is approximately 2), the effective radius is related in a

simple manner to the optical thickness and the ice water path, $r_e = \frac{3}{2\rho}\frac{w}{\tau}$ where w is the ice water path, τ is the optical thickness, and ρ is the density of water. In the case of spherical particles, the effective radius that is calculated with this relationship has a direct physical connection to the size distribution. In the case of nonspherical particles, the interpretation is more complicated. For the satellite algorithms, the retrieved effective radius can be expressed as $r_e = \frac{3}{4}\frac{V}{A_{pro}}$ and interpreted as the ratio of the volume of ice V (or by way of the solid ice density to the condensed mass) to the cross sectional area (A_{pro}). This cross sectional area is a habit-dependent parameter that complicates the interpretation of the effective radius as a simple ratio of distribution moments. For MOD06, the retrieval algorithm assumes a mixture of habits whose fractional abundances depend on particle size (King et al., 2003). For a particular habit, A_{pro} is given by the empirical dimensional power laws reported in Mitchell (1996), i.e. $A_{pro} = a_A D^{b_A}$ where D is maximum dimension. The MOD06 retrieval algorithm is described in Platnick et al. (2003). The MODIS-CERES particle sizes are based entirely on varying distributions of solid hexagonal ice columns of varying lengths (L) and widths (D). The effective radius reported here is the effective diameter D_e (Minnis et al. 1998) divided by 2. The value of D_e is the same as that defined by Ou et al. (1993): $D_e = \int D^2 Ln(L)dL / \int DLn(L)dL$. A constant density of 0.9 g cm^{-3} is used for all crystals.

The complicating factors in comparing the particle sizes arise from the effective density relationship used in the Z-Radiance algorithm and the projected area relationships used in the MOD06 retrieval. If we assume that the water paths retrieved by the two algorithms are equal, it is easy to show that $r_{e,MODIS} = \pi \frac{\left\langle a_s^2 \right\rangle r_{e,gnd}}{A_{pro}}$ where $\left\langle a_s^2 \right\rangle$ represents the second moment of the solid-equivalent size distribution (denoted by the subscript s); $N(D_s) = N_x \exp(\alpha_s)\left(\frac{D_s}{D_{x,s}}\right)^{\alpha_s} \exp\left[\frac{\alpha_s D_s}{D_{x,s}}\right]$. This modified gamma size distribution described by Mace et al. (1998) is derived in terms of the number of particles per unit length per unit volume at the functional maximum (N_x), the diameter of the solid particles

at the functional maximum, $D_{x,s}$, and the order of the solid-equivalent gamma distribution, α_s. With the Brown and Francis approximation of bulk density and an assumption that the order of the retrieved distribution (α – note the lack of subscript *s*) is unity, the Z-Radiance algorithm calculates N_x and D_x from the radar reflectivity and downwelling thermal infrared radiance (See Appendix A). To convert to a solid-equivalent size distribution, we assume that the total number of particles, N_T, and the ice water content, *iwc*, are the same between the two distributions. We assume that N_x is the same also requiring us to calculate α_s and $D_{x,s}$. With $\rho_{eff} = a_\rho D^{b_\rho}$, we can integrate the size distributions to derive the *iwc* and equate the two resulting expressions to arrive at

$$\rho_{ice} e^{\alpha_s} D_{x,s}^4 \frac{\Gamma\left(4+\alpha_s\right)}{\alpha_s^{4+\alpha_s}} = e^1 a_\rho C D_x^{4+b_\rho} \Gamma\left(5+b_\rho\right). \tag{B1}$$

In equation (B1), the left hand side of the equation results from an assumption of solid particles with ρ_{ice}=0.92 g cm^{-3} while the right hand side assumes an effective density relationship adapted from figure 3 of Brown and Francis (1995) where $a_\rho = 121.6$ and $b_\rho = -1.08$ (cgs units). The effective density power law relationship is strictly applicable only for particles with a maximum dimension larger than 100 μm although equation (B1) is derived by integrating over all sizes. A size-dependent correction factor (*C*) is derived to account for this. In equation (B1), a common factor, $\frac{N_x \pi}{6}$, has been cancelled from the right and left sides. Using similar assumptions, we can equate the total particle concentration of the solid equivalent and retrieved distributions,

$$\frac{D_{x,s} e^{\alpha_s} \Gamma\left(\alpha_s + 1\right)}{\alpha_s^{\alpha_s+1}} = D_x e^1 \tag{B2}$$

where a common factor N_x has been cancelled from both sides. Solving, equation (B2) for $D_{x,s}$ and substituting into equation (B1), α_s is derived using a straightforward minimization technique, and $D_{x,s}$ is then easily determined.

With an approximate description of the solid-equivalent size spectrum, we are in a position to calculate $\left\langle a_s^2 \right\rangle = \frac{N_x e^{\alpha_s}}{8 D_{x,s}} \int D^{2+\alpha_s} \exp\left(\frac{-D\alpha_s}{D_{x,s}}\right) dD$ where $2a = D$ is used to

convert variables in the integration. Finally, A_{pro} is calculated with the fractional abundances of the various habits as follows,

$$A_{pro} = \frac{N_x e^1}{D_x^{\alpha}} \sum_{i}^{habits} a_{A,i} f_i \int D^{b_{A,i}+1} \exp\left(\frac{-D}{D_x}\right) dD . \quad \text{(B3)}$$

In equation (B3), the integration is conducted using the retrieved size spectrum (i.e. N_x, $D_{x,}$, α=1) because the Mitchell (1996) area-dimensional relations are defined in terms of the particle maximum dimension. Following King et al., (2003), $a_{A,i}$, $b_{A,i,}$ and f_i correspond to the various habits. For particles less than 70 μm, f_i has values of 0.5 for bullet rosettes, 0.25 for hexagonal columns, and 0.25 for plates. When D>70 μm, f_i is 0.3 for aggregates, 0.3 for bullet rosettes, 0.2 for columns and 0.2 for plates.

Figure B1 shows the ratio of $r_{e,MOD06}$ to $r_{e,gnd}$ plotted as a function of $r_{e,gnd}$. We find, as expected, that $r_{e,MOD06}$ is always smaller than that retrieved assuming an ice effective density lower than solid ice and that the effect is largest at the smallest particle sizes. Given that the effective density is smallest at the largest particle sizes, one might expect that the disparity between the MOD06 definition of effective radius and the ground-based retrieval would be largest at the largest sizes. However, the cross sectional area assumed by MOD06 increases less rapidly compared to a spherical particle and there is a tradeoff between the slower increase of cross sectional area to the more rapid increase of $\left\langle a_s^2 \right\rangle$ for a given size. While the conversion function is monotonic, its rate of change varies with size in the 30-50 μm range due to the different particle habit weighting of the MOD06 A_{pro}.

Acknowledgements: This research would not have been possible without substantial assistance from several individuals on the MODIS Atmospheres and CERES science teams including Dr. William Ridgway who provided access to MODIS data and products. Mr. Michael Poellot and the University of North Dakota Citation team worked hard during several field campaigns at the ARM SGP site. Data were obtained from the Atmospheric Radiation Measurement Program sponsored by the U. S. Department of Energy, Office of Science, Office of Biological and Environmental Research, Environmental Science Division. Specifically, we would like to thank Mr. Jim Teske and staff at the SGP site for keeping the instruments functioning and the data flowing in a

sometimes challenging environment. Primary funding for this work was provided by a NASA EOS Validation Program grant (NAG56458), by the Environmental Science Division of the U. S. Department of Energy (Grant DE-FG0398ER62571). P.Y. was supported in this work by NSF grant (ATM-0239605) and NASA grant (NAG-1-02002). The CERES MODIS retrieval results were provided by Sunny Sun-Mack and developed with support by the NASA Earth System Enterprise through the CERES Project. Additional support provided by the U.S. Department of Energy via Interagency Agreement DE-AI02-97ER62341.

References:

Ackerman, T. P., K. N. Liou, F. P. J. Valero, and L. Pfister, 1988: Heating rates in tropical anvils. *J. Atmos. Sci.*, **45**, 1606-1623.

Brown, P. R. A., and P. N. Francis, 1995: Improved measurements of the ice water content in cirrus using a total water probe. *J. Atmos. Oceanic Technol.*, **11**, 410-414.

Comstock, J. M., T. P. Ackerman, and G. G. Mace, 2002: Ground-based lidar and radar remote sensing of tropical cirrus clouds at Nauru Island: Cloud statistics and radiative impacts. *J. Geophys. Res.*, **107** (D23), 4714, doi:10.1029/2002JD002203.

Cox, S. K., 1971: Cirrus clouds and climate. *J. Atmos. Sci.*, **28**, 1513-1515.

Dong, X., and G. G. Mace, 2003: Profiles of low-level stratus cloud microphysics deduced from ground-based measurements. *J. Atmos. Oceanic. Technol.*, **20**, 42-53.

Dowling, D. R., and L. F. Radke, 1990: A summary of the physical properties of cirrus clouds, *J. Appl. Meteor.*, **29**, 970-978.

Fu, Q., and K. N. Liou, 1993: Parameterization of the radiative properties of cirrus clouds. *J. Atmos. Sci.*, **50**, 2008-2025.

Fu, Q., 1996: An accurate parameterization of the solar radiative properties of cirrus clouds for climate models. *J. Climate*, **9**, 2058-2082.

Fu, Q., P. Yang and W. B. Sun, 1998: An accurate parameterization of the infrared radiative properties of cirrus clouds for climate models. *J. Climate*, **11**, 2223-2237.

Gao, B. C., and Y. J. Kaufman, 1995: Selection of the 1.375-μm MODIS channel for remote sensing of cirrus clouds and stratospheric aerosols from space. *J. Atmos. Sci.*, **52**, 4231-4237.

Gao, B. C., A. F. Goetz, and W. J. Wiscombe, 1993: Cirrus cloud detection from airborne imaging spectrometer data using the 1.38 μm water vapor band. *Geophys. Res. Lett*., **20**, 301-304.

Gossard, E. E., 1994: Measurement of cloud droplet size spectra by Doppler radar. *J. Atmos. Oceanic Technol.*, **11**, 712-726.

Heymsfield, A. J., and C. M. R. Platt, 1984: A parameterization of the particle size spectrum of ice clouds in terms of the ambient temperature and the ice water content. *J. Atmos. Sci.*, **41**, 846-855.

Heymsfield, A. J., and J. L. Parrish, 1986: Interactive system for processing PMS two-dimensional imaging probe data. *J. Atmos. Oceanic. Technol.*, **3**, 734-739.

King, M. D., and D. D. Herring, 2000: Monitoring Earth's vital signs. *Sci. Amer*., **282**, 72-77.

King, M. D., Y. J. Kaufman, W. P. Menzel and D. Tanré, 1992: Remote sensing of cloud, aerosol, and water vapor properties from the Moderate Resolution Imaging Spectrometer (MODIS). *IEEE Trans. Geosci. Remote Sens.*, **30**, 2-27.

King, M. D., Si-Chee Tsay, S. E. Platnick, Menghua Wang, and K. N. Liou, 1997: Cloud retrieval algorithms for MODIS: optical thickness, effective particle radius, and thermodynamic phase.

King, M. D., W. P. Menzel, Y. J. Kaufman, D. Tanr B. C. Gao, S. Platnick, S. A. Ackerman, L. A. Remer, R. Pincus, and P. A. Hubanks, 2003: Cloud and Aerosol Properties, Precipitable Water, and Profiles of Temperature and Humidity from MODIS. IEEE Trans. Geosci. Remote Sens., 41, 442-458.

King, M. D., S. Platnick, P. Yang, G. T. Arnold, M. A. Gray, J. C.Riédi, S. A. Ackerman, and K. N. Liou, 2003: Remote sensing of liquid water and ice cloud optical thickness, and effective radius in the arctic: Application of air-borne multispectral MAS data. *J. Atmos. Sc.*. (submitted)

Liou, K. N., 1986: Influence of cirrus clouds on weather and climate processes: A global perspective. *Mon. Wea, Rev.*, **114**, 1167-1199.

Lynch, D. K., K. Sassen, D. O'C. Starr, and G. Stephens (Eds.). Cirrus (Oxford Univ. Press, New York, 2002).

Manabe, S., and R. T. Wetherald, 1967: Thermal equilibrium of the atmosphere with a given distribution of relative humidity. *J. Atmos. Sci.*, **24**, 241-259.

Mace, G. G., T. P. Ackerman, and E. E. Clothiaux, 1997: A study of composite cirrus morphology using data from a 94-GHz radar and correlations with temperature and large-scale vertical motion. *J. Geophys. Res.*, **102**, 13581-13593.

Mace, G. G., T. A. Ackerman, P. Minnis, and D. F. Young, 1998: Cirrus layer microphysical properties derived from surface-based millimeter radar and infrared interferometer data. *J. Geophys. Res.*, **103**, 23027-23216.

Mace, G. G., E. E. Clothiaux, and T. A. Ackerman, 2001: The composite characteristics of cirrus clouds: Bulk properties revealed by one year of continuous cloud radar data. *J. Climate*, **14**, 2185-2203.

Mace, G. G., A. J. Heymsfield, and Michael R. Poellot, 2002: On retrieving the microphysical properties of cirrus clouds using the moments of the millimeter-wavelength Doppler spectrum. *J. Geophys. Res.*, **107**, 4815-4841.

Mace, G. G., 2003: On retrieving the microphysical properties of cirrus clouds using the moments of the millimeter-wavelength doppler spectrum: Part II An analytical framework and formal error analysis. *J. Geophys. Res.*, in press.

Minnis, P., D. P. Garber, D. F. Young, R. F. Arduini, and Y. Takano, 1998: Parameterization of reflectance and effective emittance for satellite remote sensing of cloud properties. *J. Atmos. Sci.*, **55**, 3313-3339.

Minnis, P., D. P. Kratz, J. A. Coakley, Jr., M. D. King, D. Garber, P. Heck, S. Mayor, D. F. Young, and R. Arduini, 1995: Cloud Optical Property Retrieval (Subsystem 4.3). "Clouds and the Earth's RadAnalyses and Radiance Inversions (Subsystem 4)", NASA RP 1376 Vol. 3, edited by CERES Science Team, pp. 135-176.

Minnis, P., D. F. Young, B. A. Weilicki, S. Sun-Mack, Q. Z. Trepte, Y. Chen, P. W. Heck, and X. Dong, 2002: A global cloud database from VIRS and MODIS for CERES. *Proc. SPIE 3rd Intl. Asia-Pacific Environ. Remote Sensing Symp. 2002: Remote Sens. of Atmos, Ocean, Environ.t, and Space*, Hangzhou, China, (At HYPERLINK "http://wwwpm.larc.nasa.gov/ceres/pub/conference/Minnis.SPIE.02.pdf" http://wwwpm.larc.nasa.gov/ceres/pub/conference/Minnis.SPIE.02.pdf)

Mitchell, D. L., 1996: Use of mass- and area-dimensional power laws for determining precipitation particle terminal velocities. *J. Atmos. Sci.*, **53**, 1710-1723.

Moran, K. P., B. E. Martner, M. J. Post, R. A. Kropfli, D. C. Welsh, and K. B. Widener, 1998: An unattended cloud-profiling radar for use in climate research. *Bull. Amer. Meteor. Soc*, **79**, 443-455.

Ou, S. C., K. N. Liou, Y. Takano, N. X. Rao, Q. Fu, A. J. Heymsfield, L. M. Miloshevich, B. Baum, and S. A. Kinne, 1995: Remote sounding of cirrus optical depths and ice crystals sizes from AVHRR data: Verification using FIRE II IFO measurements. *J. Atmos. Sci.*, 52, 4143-4158

Platnick, S., M. D. King, S. A. Ackerman, W. P. Menzel, B. A. Baum, J. C.Riédi, and R. A. Frey, 2003: The MODIS Cloud Products: Algorithms and Examples from Terra. *IEEE Trans. Geosci. Remote Sens.*, **41**, 459-473.

Poellot, M. R., K. A. Hilburn, W. P. Arnott, and K. Sassen, 1999: In situ observations of cirrus clouds from the 1994 ARM RCS IOP. In *Ninth ARM Science Team Meeting Proceedings*, San Antonio, Texas, March 22-26, 1999.

Rossow, W. B., and R. A. Schiffer, 1999: Advances in understanding clouds from ISCCP. *Bull. Amer. Meter. Soc*., **80**, 2261-2286.

Sassen, K., and J. R. Campbell, 2001: A midlatitude cirrus cloud climatology from the facility for atmospheric remote sensing. Part I: Macrophysical and synoptic properties. *J. Atmos. Sci.*, **58**, 481–496.

Sassen, K., Z. Wang, C.M.R. Platt, and J.M. Comstock, 2003: Parameterization of infrared absorption in midlatitude cirrus clouds. *J. Atmos. Sci.*, **60**, 428-433.

Smith, W. L., S. Ackerman, H. Revercomb, H. Huang, D. H. DeSlover, W. Feltz, L. Gumley, and A. Collard, 1998: Infrared spectral absorption of nearly invisible cirrus clouds. *Geophys. Res. Lett.*, **25**, 1137-1140.

Stephens, G. L., and P. J. Webster, 1981: Clouds and climate: Sensitivity of simple systems. *J. Atmos. Sci.*, **38**, 235-247.

Stephens, G. L., S.-C. Tsay, P. W. Stackhouse, Jr., and P. J. Flatau, 1990: The relevance of the microphysical and radiative properties of cirrus clouds to climate and climatic feedback. *J. Atmos. Sci.,* **47,** 1742–1753.

Spinhirne, J. D., and W. D. Hart, 1990: The 27-28 October 1986 FIRE cirrus case study: Cirrus structure and radiative parameters from airborne lidar and spectral radiometer observations. *Mon. Wea. Rev.*, **118**, 2329-2343.

Stokes, G. M., and S. E. Schwartz, 1994: The Atmospheric Radiation Measurement (ARM) Program: programmatic background and design of the cloud and radiation test bed. *Bull. Amer. Meteor. Soc.*, **75**, 1201-1221.

Weickmann, H. K., 1948: Die Eisphase in der Atmosphare. Royal Aircraft Establishment, 96 pp.

Webster, P. J., 1994: The role of hydrological processes in ocean-atmosphere interactions. *Rev. Geophys.*, **32**, 427-476.

Wylie, D. P., and W. P. Menzel, 1989: Two years of cloud cover statistics using VAS. *J. Clim.*, **2**, 380-392.

Wylie, D. P., W. P. Menzel, H. M. Woolf, and K. I. Strabala, 1994: Four years of global cirrus cloud statistics using HIRS. *J. Climate*, **7**, 1972-1986.

Wylie, D. P., and W. P. Menzel, 1999: Eight years of high cloud statistics using HIRS. *J. Climate*, **12**, 170-184.

Zhang, Yuying, 2002: On the use of ground-based, aircraft and satellite data for the study of cirrus clouds. *M.S. Thesis*, Univ. of Utah, pp. 133.

Tables

Table 1. Summary of the properties retrieved from data collected on 6 March 2001. Shown are the mean and standard deviation of the properties observed in the rectangular region depicted in Figure 1 for the MOD06 and MODIS-CERES retrievals and in the time series of properties from the ground-based Z-Velocity algorithm shown in Figure 4.

	Z-Velocity	MOD06	MODIS-CERES
r_e (μm)	30.3/1.7	29.9/2.2	31.2/3.1
IWP (g/m^2)	54.0 / 12.7	61.8 / 16.2	59.1 / 18.0
Optical Depth	2.02 / 0.34	2.78 / 0.68	3.08 / 0.83
Cloud Top Temperature (K)	216.2 / 2.2	237.6 / 3.6	
Cloud Top Pressure (hPa)	236.7 / 8.8	359.3 / 28.2	307.7 / 24.5

Table 2. Dates and times of the MODIS data used in the thin cirrus intercomparison. The * denotes Terra cases for which MODIS-CERES cloud analysis has also been performed.

Date (yyyymmdd)	Overpass Time (UTC)	Viewing Angle (°)
*20001127	17:07:14	47.8
*20001128	17:49:55	24.1
*20001130	17:37:39	1.0
*20001220	17:13:04	40.5
20010322	17:35:28	2.1
*20010330	16:46:25	62.9
20010330	18:24:04	62.9
*20010527	17:22:05	21.4
*20010606	17:58:23	42.2
*20010903	17:50:03	34.4
20010904	16:54:58	53.3
20011125	16:40:07	62.7
20011125	18:17:45	63.1
*20011221	17:15:43	22.1
20011228	17:21:45	10.6

Table 3. Statistics of the comparison of thin cirrus properties shown in Figure 12. Shown here are the linear correlation coefficient, the slope of a best fit linear regression line, the mean bias, and the standard deviation of the mean bias compared with the Z-Radiance ground-based retrievals.

	Property	Linear Correlation Coefficient	Slope	Mean Bias	Bias Standard Deviation
MOD06	r_e (μm)	0.424	0.406	1.45	8.16
	IWP (g/m^2)	0.694	1.344	13.13	39.01
	Optical Depth	0.571	1.068	0.79	1.59
	Cloud Top Height (km)	0.809	0.854	-0.586	1.29
MODIS-CERES	r_e (μm)	0.678	0.548	-2.925	6.45
	IWP (g/m^2)	0.763	0.946	-3.345	16.19
	Optical Depth	0.838	1.164	0.210	0.83
	Cloud Top Height (km)	0.592	0.348	-2.482	1.15

Table 4. The number of observations used as a function of visible optical depth used in the statistical comparisons shown in Figures 15-18.

τ	<0.5	0.5~1.0	1.0~1.5	1.5~2.0	2.0~3.0	3.0~4.0	4.0~5.0
MOD06 pixels	811	2036	160,378	93,496	189,675	159,460	142,582
ARM SGP points	3131	1003	522	287	331	205	123

Table A.1 Coefficients and exponents to mass-dimensional power laws for various ice crystal types. Random orientation is assumed for D < 100 μm, horizontal orientation otherwise (adapted from Mitchell 1996).

Particle type	α	β	References
Hexagonal plates 100 ~3000 μm	0.00739	2.45	Mitchell and Arnott (1994), Mitchell et al. (1996), Auer and Veal (1970)
Hexagonal columns 100 ~300 μm	0.00166	1.91	Mitchell and Arnott (1994), Mitchell et al. (1996), Auer and Veal (1970), Heymsfield and Knollenburg (1972)
300 μm and up	0.000907	1.74	
Crystal with sector-like branches 40~2000 μm	0.00142	2.02	Mitchell and Arnott (1994), Mitchell et al. (1996), Auer and Veal (1970), Pruppacher and Klett (1978)
Broad-branched crystal 100 ~1000 μm	0.000516	1.8	Pruppacher and Klett (1978), Mitchell et al. (1996)
Side plates 300~2500 μm	0.00419	2.3	Mitchell et al. (1990), Mitchell et al. (1996)
Bullet rosettes, 5 branches at 231 K 200~1000 μm	0.00308	2.26	Mitchell (1994), Mitchell et al. (1996)
Aggregates of side planes, columns and bullets 800~4500 μm	0.0028	2.1	Mitchell et al. (1990), Mitchell et al. (1996)

Figure Captions.

Figure 1. (a) Height-Time cross section of radar reflectivity observed by the MMCR at the ARM SGP site on 6 March 2001. Time is shown in UTC hours. (b) Visible image of cirrus observed by MODIS at 1735 UTC in the vicinity of the ARM SGP on 6 March 2001. The SGP central facility is shown with the light green square. The yellow lines show latitude and longitude. The image is created by combining 3 visible channels to create a near true color composite.

Figure 2. Wind profiler data observed by the NOAA 404 MHz wind profiler near Lamont Oklahoma on 6 March 2001. Observations at different times are shown by the symbols.

Figure 3. Comparison of cloud properties retrieved by the Z-Velocity algorithm applied to MMCR data collected at the SGP site and the MOD06 cloud properties retrieved using data collected on 6 March 2001 from within the rectangular region shown in Figure 2. a) shows effective particle radius, b) shows the ice water path and c) shows the optical thickness

Figure 4. As in Figure 4 except the Z-Velocity results are compared to cirrus properties derived from the MODIS-CERES algorithm.

Figure 5. As in Figure 4 except the MOD06 algorithm is compared with the MODIS-CERES results.

Figure 6. Comparison between cloud top (a) temperature and (b) pressure measured by the MMCR and local radiosonde data and that reported in the MOD06 product.

Figure 7. MMCR height-time cross section of radar reflectivity factor observed on 22 March 2001 at the ARM SGP site.

Figure 8. Layer-averaged cloud properties retrieved by the Z-Radiance algorithm using data collected on 22 March 2001.

Figure 9. (a) MODIS 1.38 micron imagery collected at 1735 UTC on 22 March 2001 over the ARM SGP site and (b) MOD06 optical thickness coincident with the field observed in (a).

Figure 10. Frequency distribution of optical depth from the MOD06 data in the vicinity of the ARM site on 22 March 2001.

Figure 11. Figure 11. Comparison of cloud top temperature and pressure reported in the MOD06 product with observations

Figure 12. Figure 12. Comparison of cirrus properties from the Z-Radiance algorithm and coincident cloud properties reported in the MOD06 product.

Figure 13. Figure 13. As in Figure 12 except the MODIS-CERES data is compared with the Z-Radiance results.

Figure 14. Figure 14. Comparison of cloud top heights reported by (a) the MOD06 product and (b) the MODIS-CERES products with observations at the ARM SGP site.

Figure 15. Figure 15. Comparison of the frequency distributions of effective radius (a) and ice water path (b) for cirrus with optical depths less than 0.5. The MOD06 properties are derived from a 100x100 km region centered on the ARM site for the period beginning in March 2000 and extending to July 2001. The Z-Radiance statistics are derived from cirrus clouds observed during this time period.

Figure 16. As in Figure 15 except for optical depths between 0.5 and 1.0

Figure 17. As in Figure 15 except for optical depths between 1.0 and 3.0

Figure 18. As in Figure 15 except for optical depths between 3.0 and 5.0

Figure A1. Sensitivity of the IWC retrieved by the Z-Radiance algorithm due to error in the input data.

Figure A2. Sensitivity of the effective radius retrieved by the Z-Radiance algorithm due to error in the input data.

Figure A3. Mass-dimensional relationships used in the calculation of IWC from aircraft data.

Figure A4. Comparison of aircraft-observed IWP and effective radius with retrieved values from the surface instruments. Due to limitations in the 2dc instrument, the observed and retrieved size distributions are integrated only over the 100-700 micron particle size range.

Figure A.5 Comparison between calculated and observed downwelling solar fluxes at the surface expressed in terms of the fraction of the downwelling solar flux removed by

cloud. (a) solar forcing calculated from Mace98 algorithm, (b) solar forcing calculated from the improved reflectivity-radiance algorithm.

Figure B1. Ratio of the effective radius definition used in the MOD06 algorithm with that used in the Z-Radiance algorithm as a function of the Z-Radiance effective radius.

Table Captions

Table 1. Summary of the properties retrieved from data collected on 6 March 2001. Shown are the mean and standard deviation of the properties observed in the rectangular region depicted in Figure 1 for the MOD06 and MODIS-CERES retrievals and in the time series of properties from the ground-based Z-Velocity algorithm shown in Figure 4.

Table 2. Dates and times of the MODIS data used in the thin cirrus intercomparison. The * denotes Terra cases for which MODIS-CERES cloud analysis has also been performed.

Table 3. Statistics of the comparison of thin cirrus properties shown in Figure 12. Shown here are the linear correlation coefficient, the slope of a best fit linear regression line, the mean bias, and the standard deviation of the mean bias compared with the Z-Radiance ground-based retrievals.

Table 4. The number of observations used as a function of visible optical depth used in the statistical comparisons shown in Figures 15-18.

Table A.1 Coefficients and exponents to mass-dimensional power laws for various ice crystal types. Random orientation is assumed for $D < 100$ μm, horizontal orientation otherwise (adapted from Mitchell 1996).

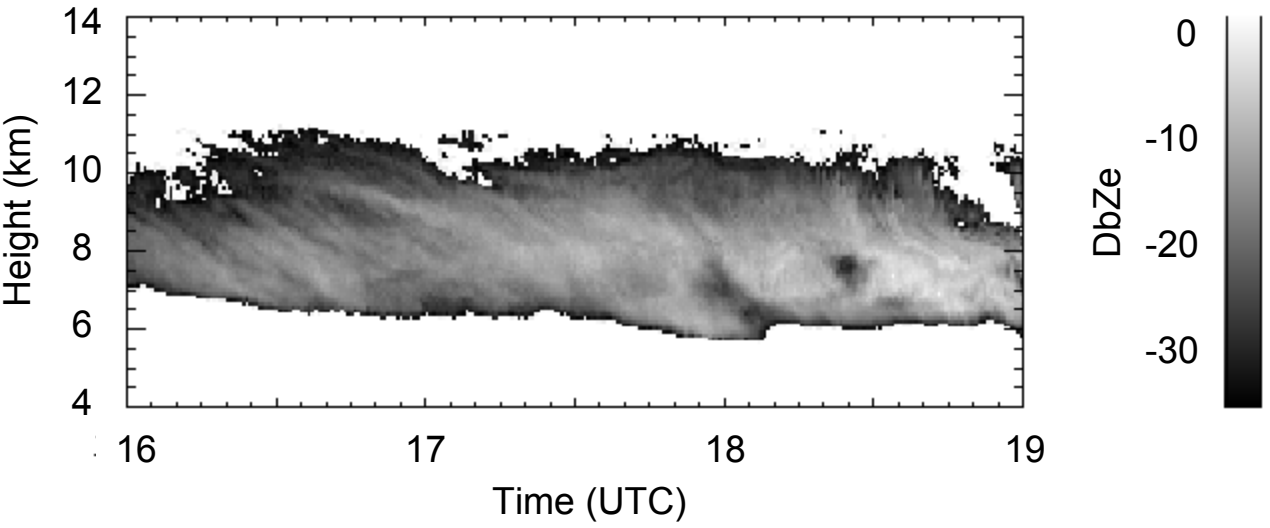

Figure 1a. Height-Time cross section of radar reflectivity observed by the MMCR at the ARM SGP site on 6 March 2001. Time is shown in UTC hours.

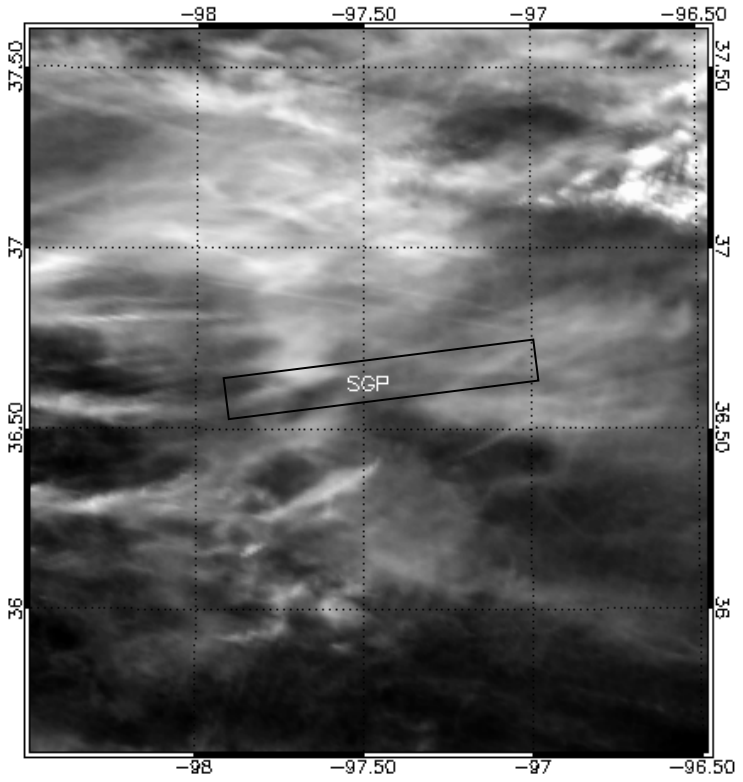

Figure 1b. Visible image of cirrus observed by MODIS at 1735 UTC in the vicinity of the ARM SGP on 6 March 2001. The SGP central facility is shown with the light green square. The yellow lines show latitude and longitude. The image is created by combining 3 visible channels to create a near true color composite.

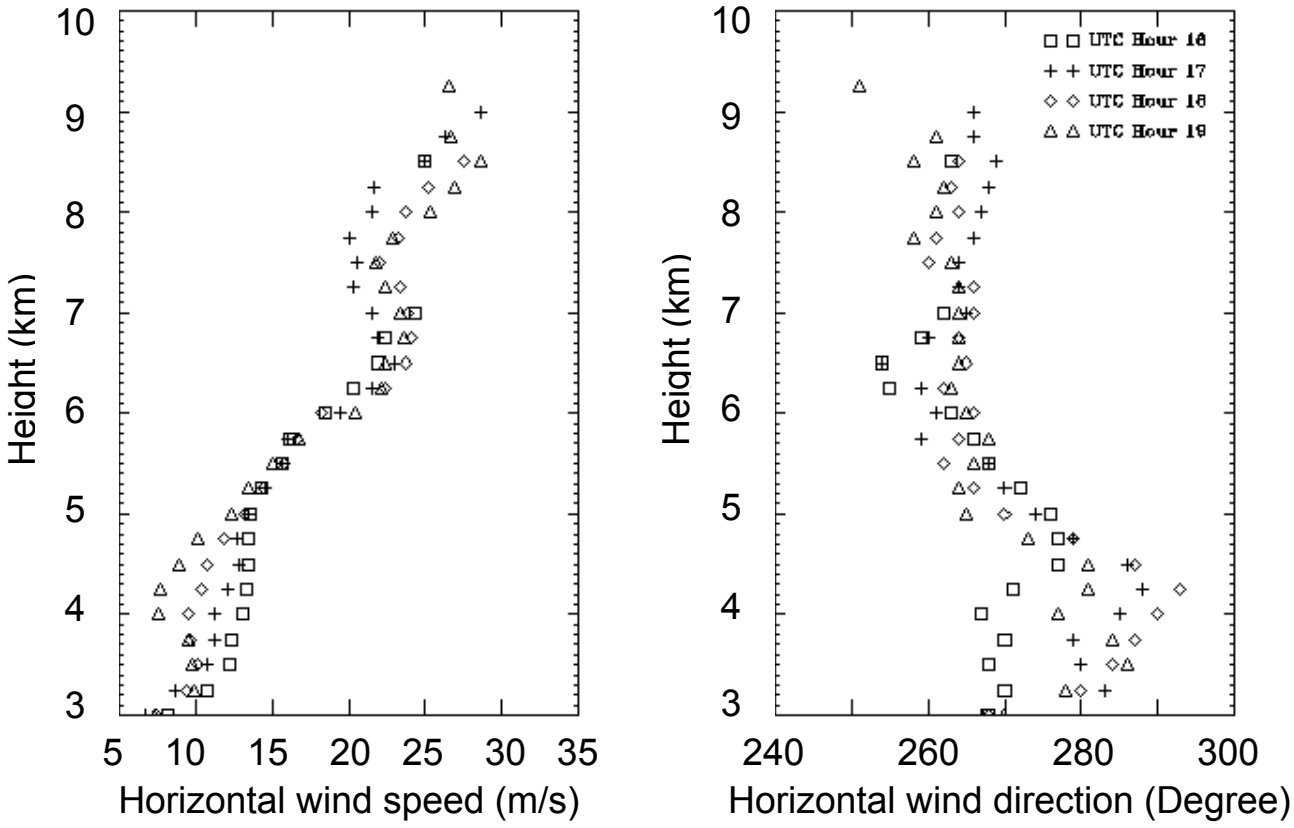

Figure 2. Wind profiler data observed by the NOAA 404 MHz wind profiler near Lamont Oklahoma on 6 March 2001. Observations at different times are shown by the symbols.

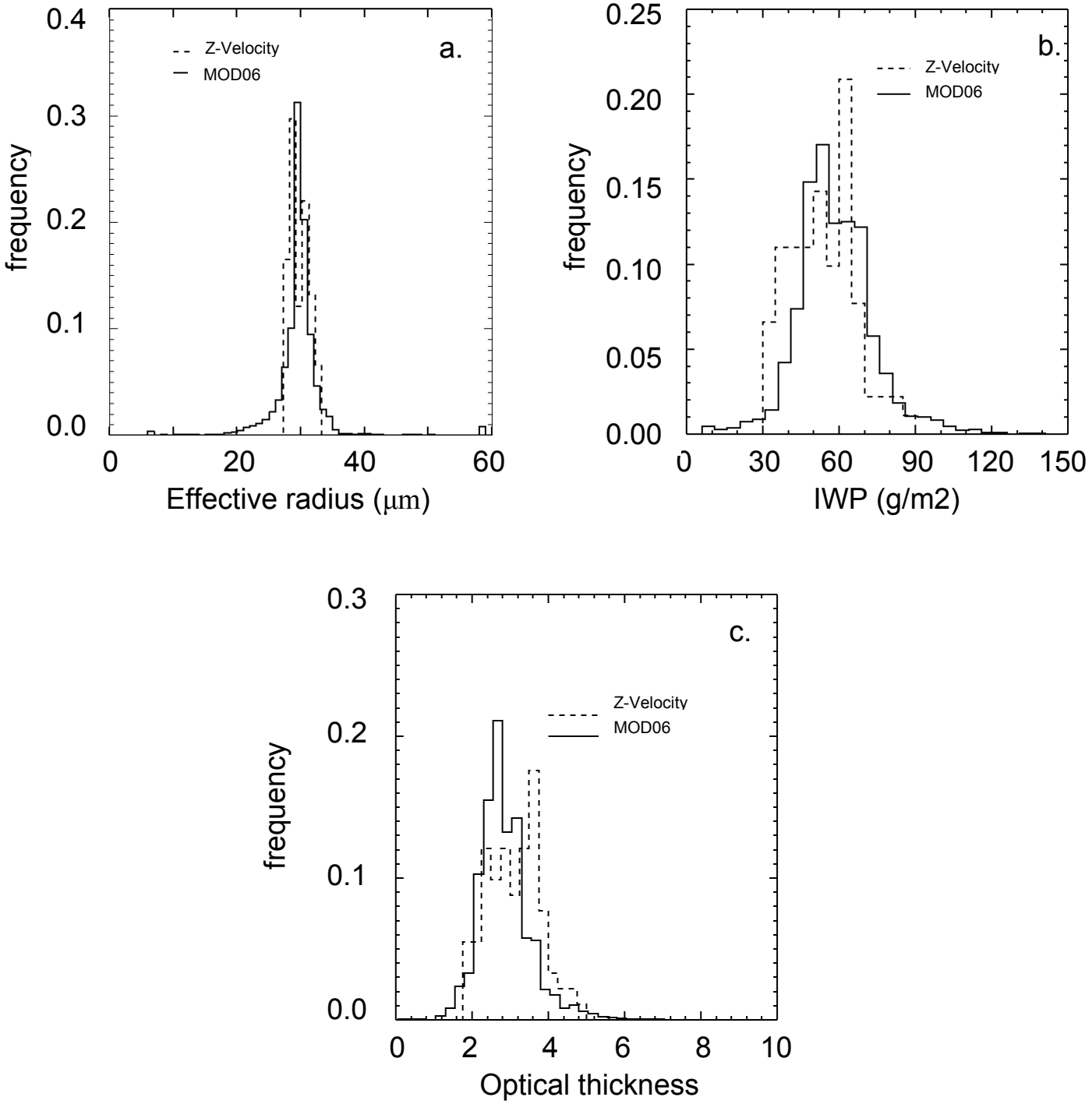

Figure 3. Comparison of cloud properties retrieved by the Z-Velocity algorithm applied to MMCR data collected at the SGP site and the MOD06 cloud properties retrieved using data collected on 6 March 2001 from within the rectangular region shown in Figure 2. a) shows effective particle radius, b) shows the ice water path and c) shows the optical thickness

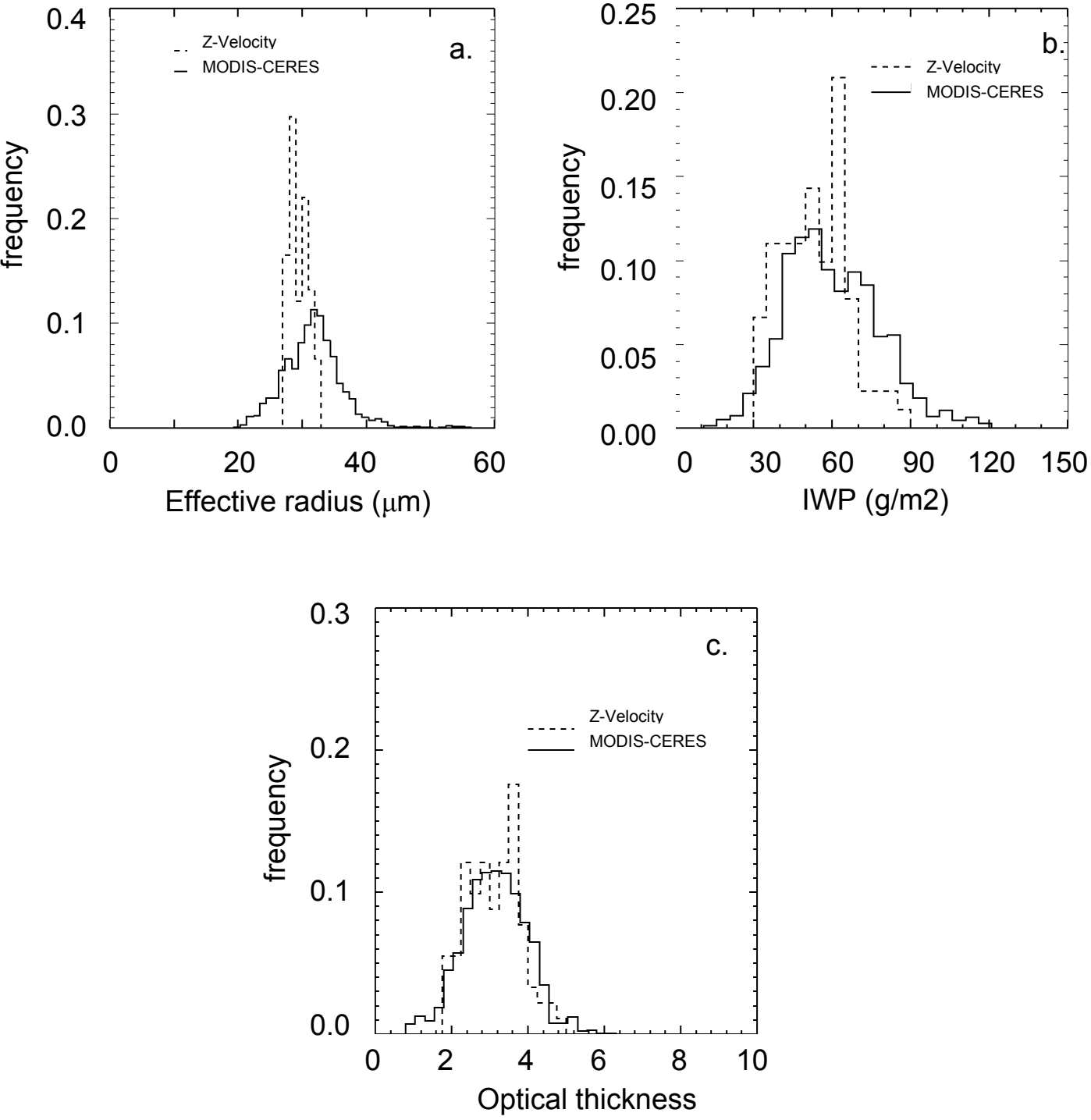

Figure 4. As in Figure 4 except the Z-Velocity results are compared to cirrus properties derived from the MODIS-CERES algorithm.

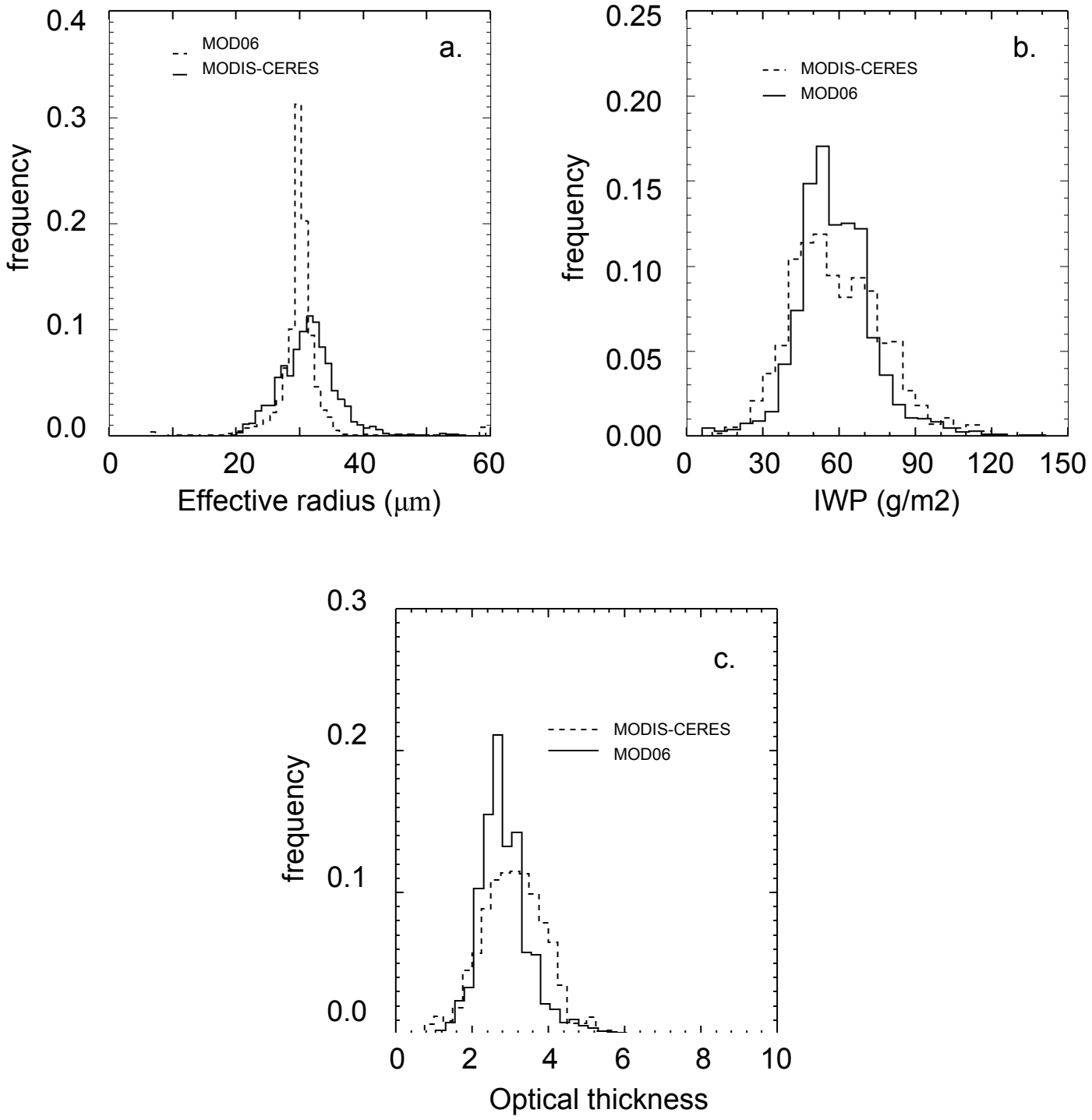

Figure 5. As in Figure 4 except the MOD06 algorithm is compared with the MODIS-CERES results.

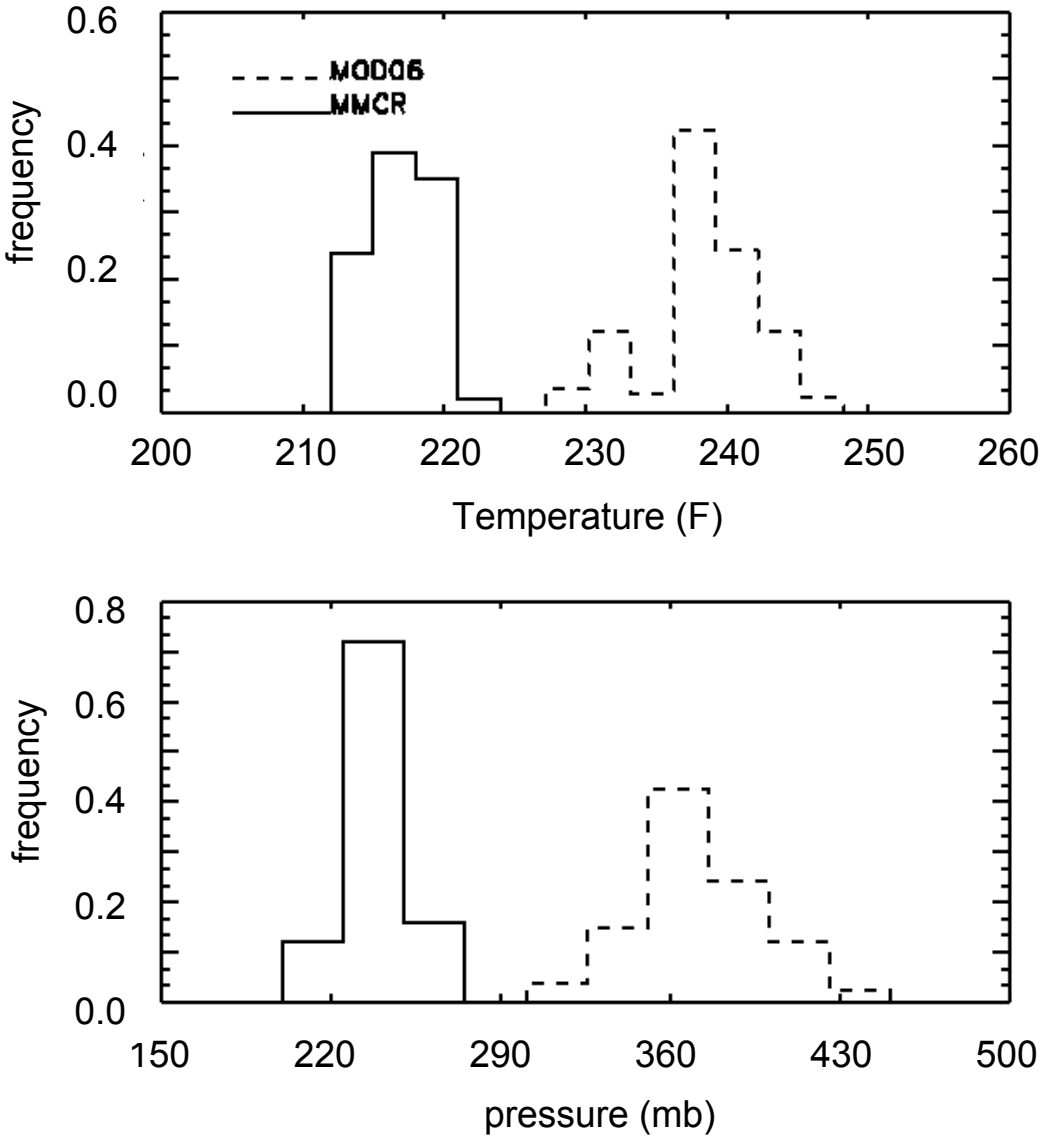

Figure 6. Comparison between cloud top (a) temperature and (b) pressure measured by the MMCR and local radiosonde data and that reported in the MOD06 product.

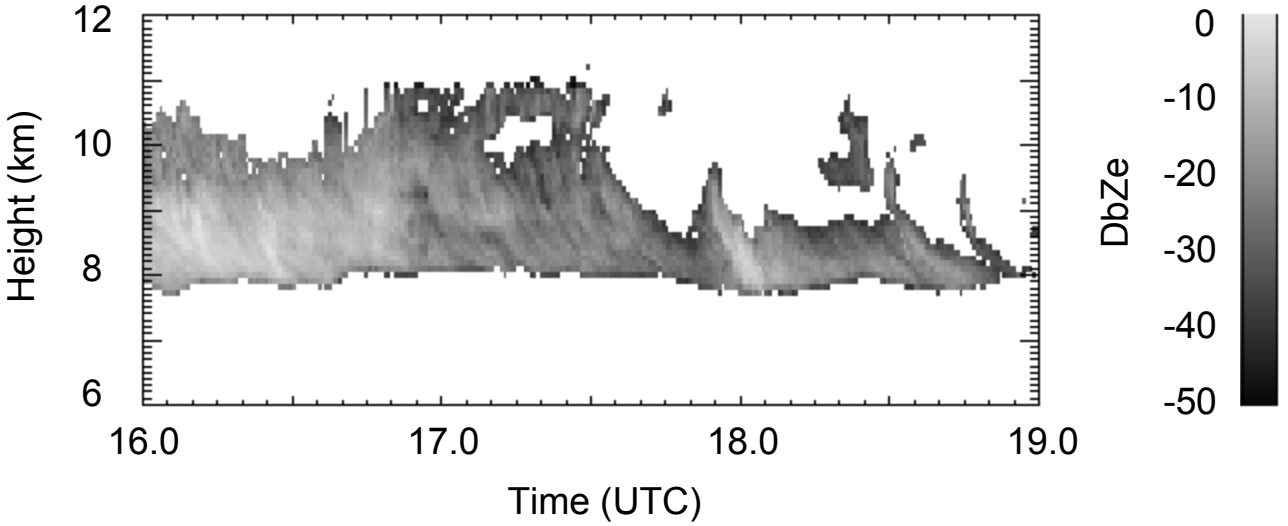

Figure 7. MMCR height-time cross section of radar reflectivity factor observed on 22 March 2001 at the ARM SGP site.

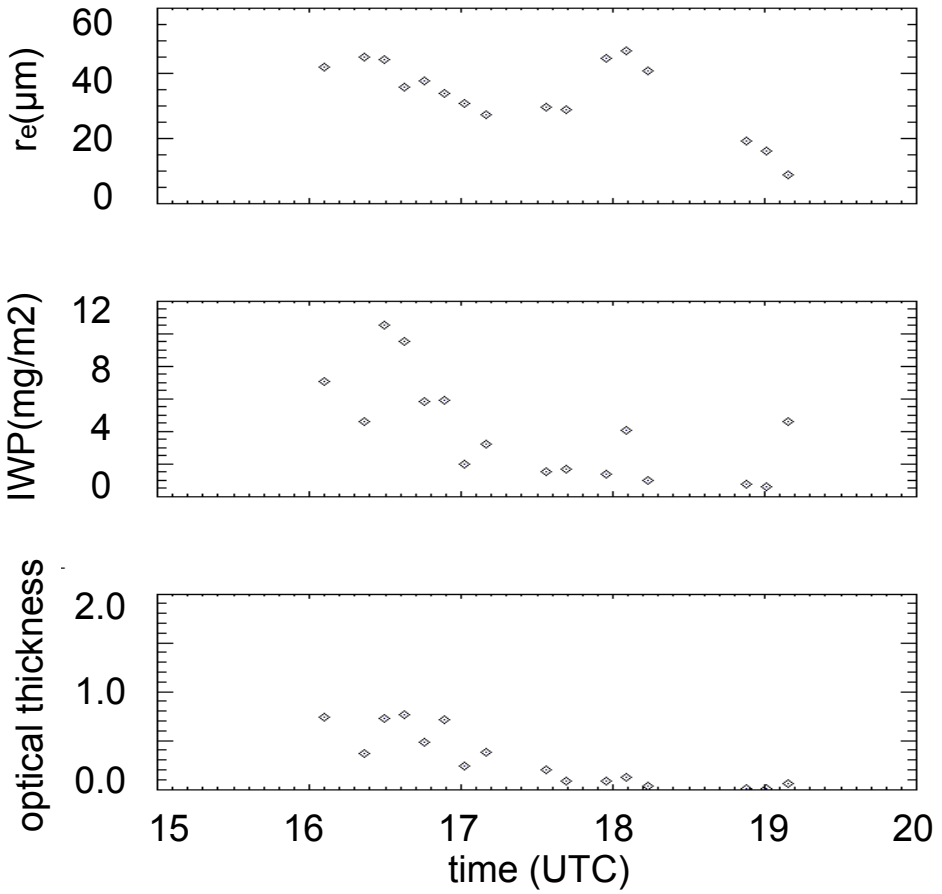

Figure 8. Layer-averaged cloud properties retrieved by the Z-Radiance algorithm using data collected on 22 March 2001.

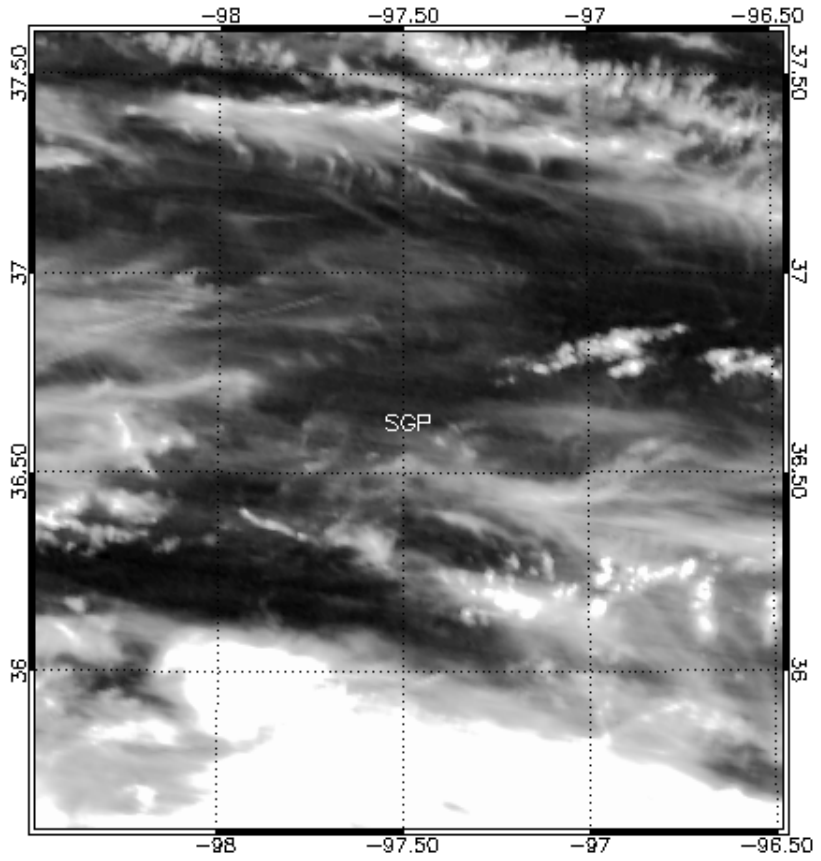

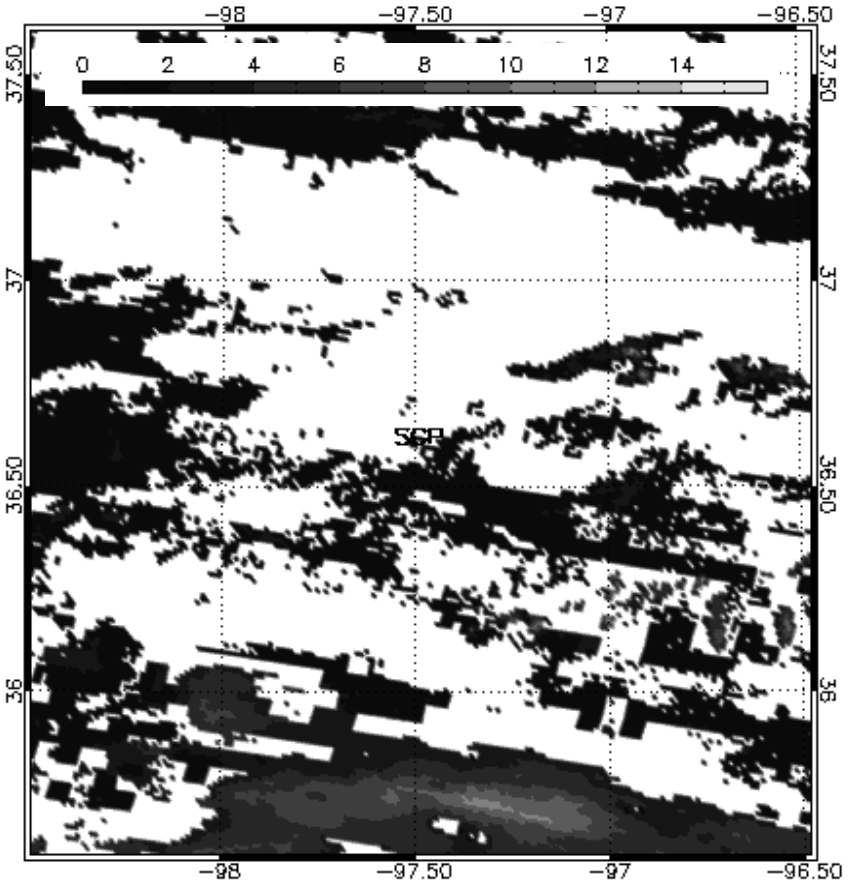

Figure 9. (a) MODIS 1.38 micro imagery collected at 1735 UTC on 22 March 2001 over the ARM SGP site and (b) MOD06 optical thickness coincident with the fiel observed in (a).

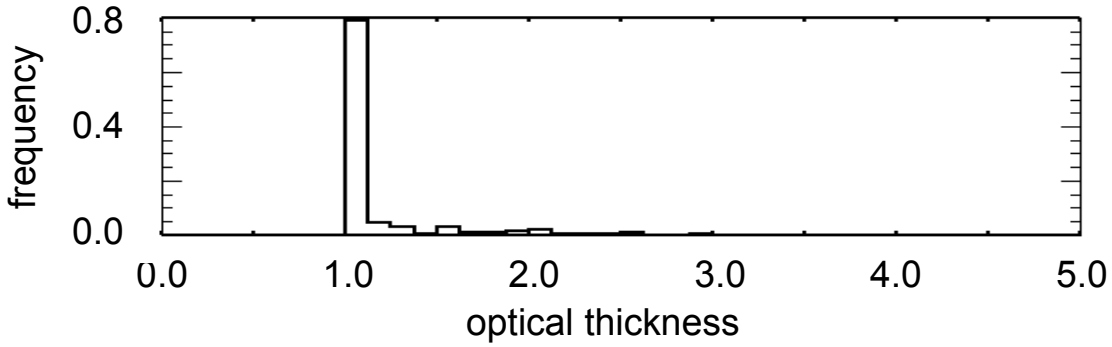

Figure 10. Frequency distribution of optical depth from the MOD06 data in the vicinity of the ARM site on 22 March 2001.

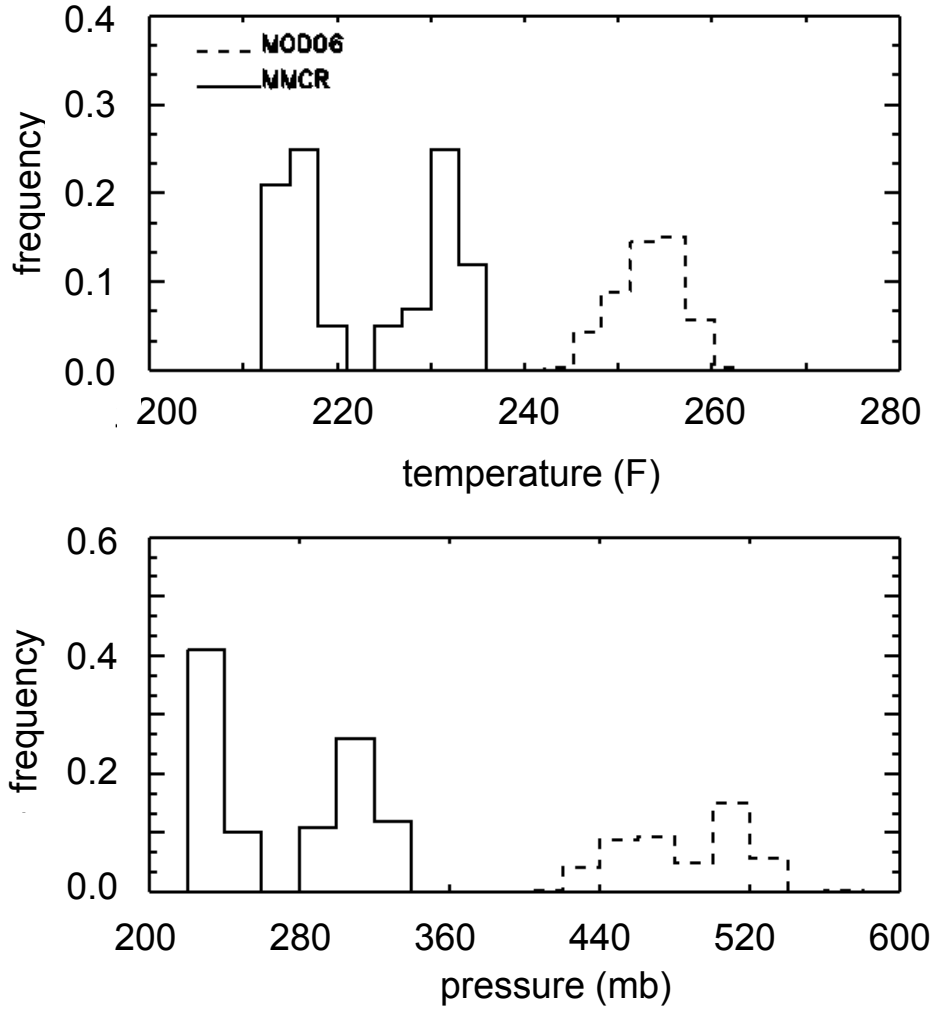

Figure 11. Comparison of cloud top temperature and pressure reported in the MOD06 product with observations

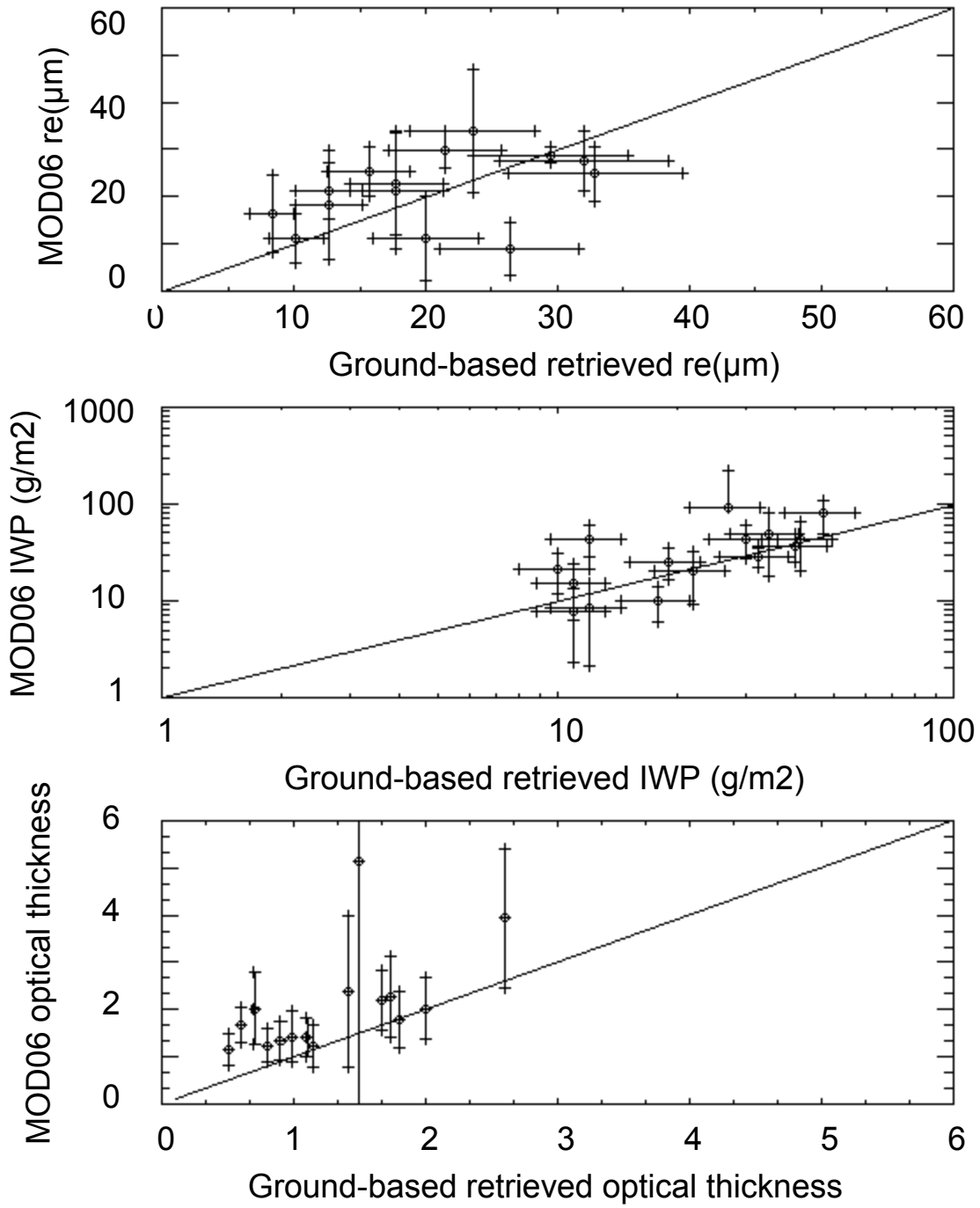

Figure 12. Comparison of cirrus properties from the Z-Radiance algorithm and coincident cloud properties reported in the MOD06 product.

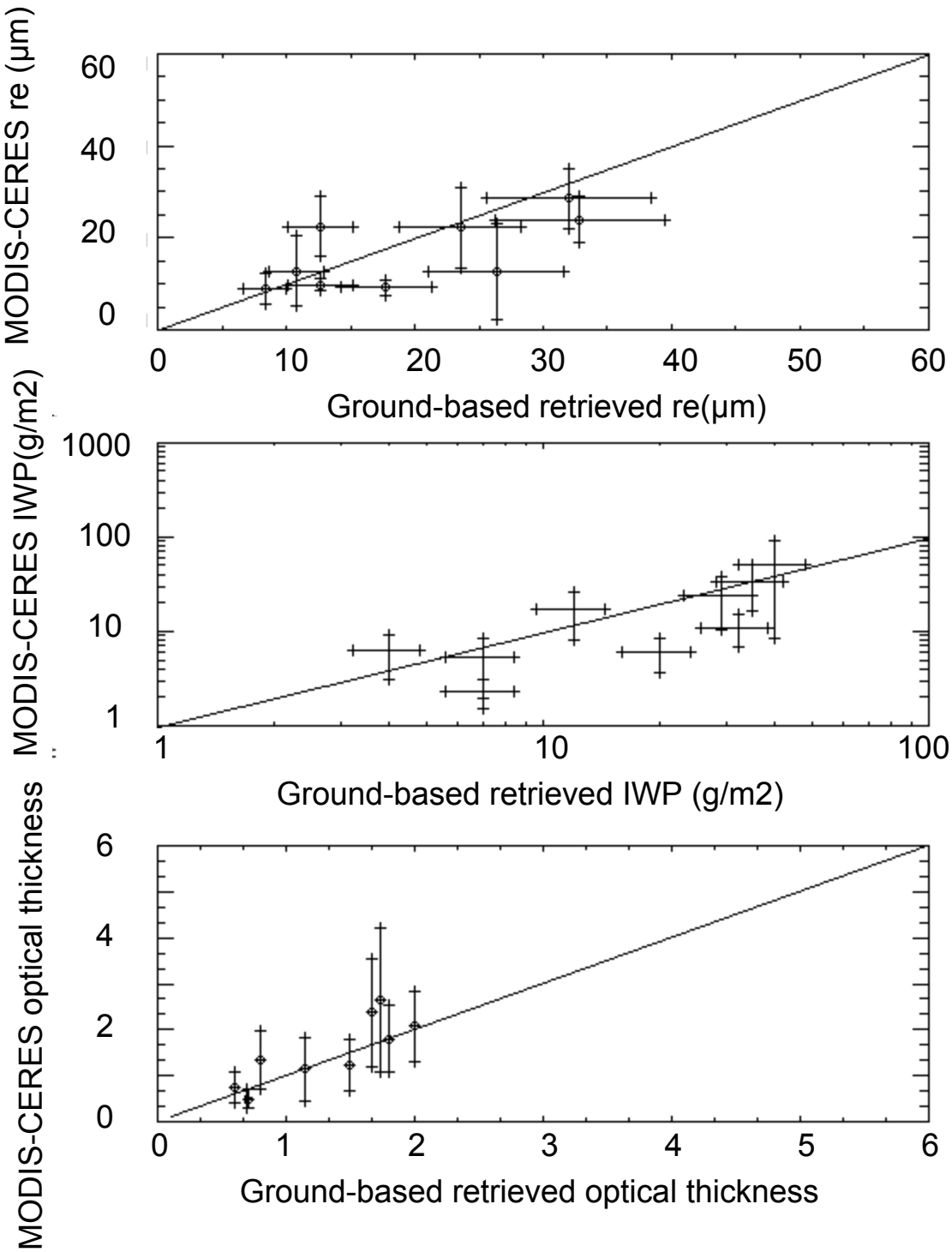

Figure 13. As in Figure 12 except the MODIS-CERES data is compared with the Z-Radiance results.

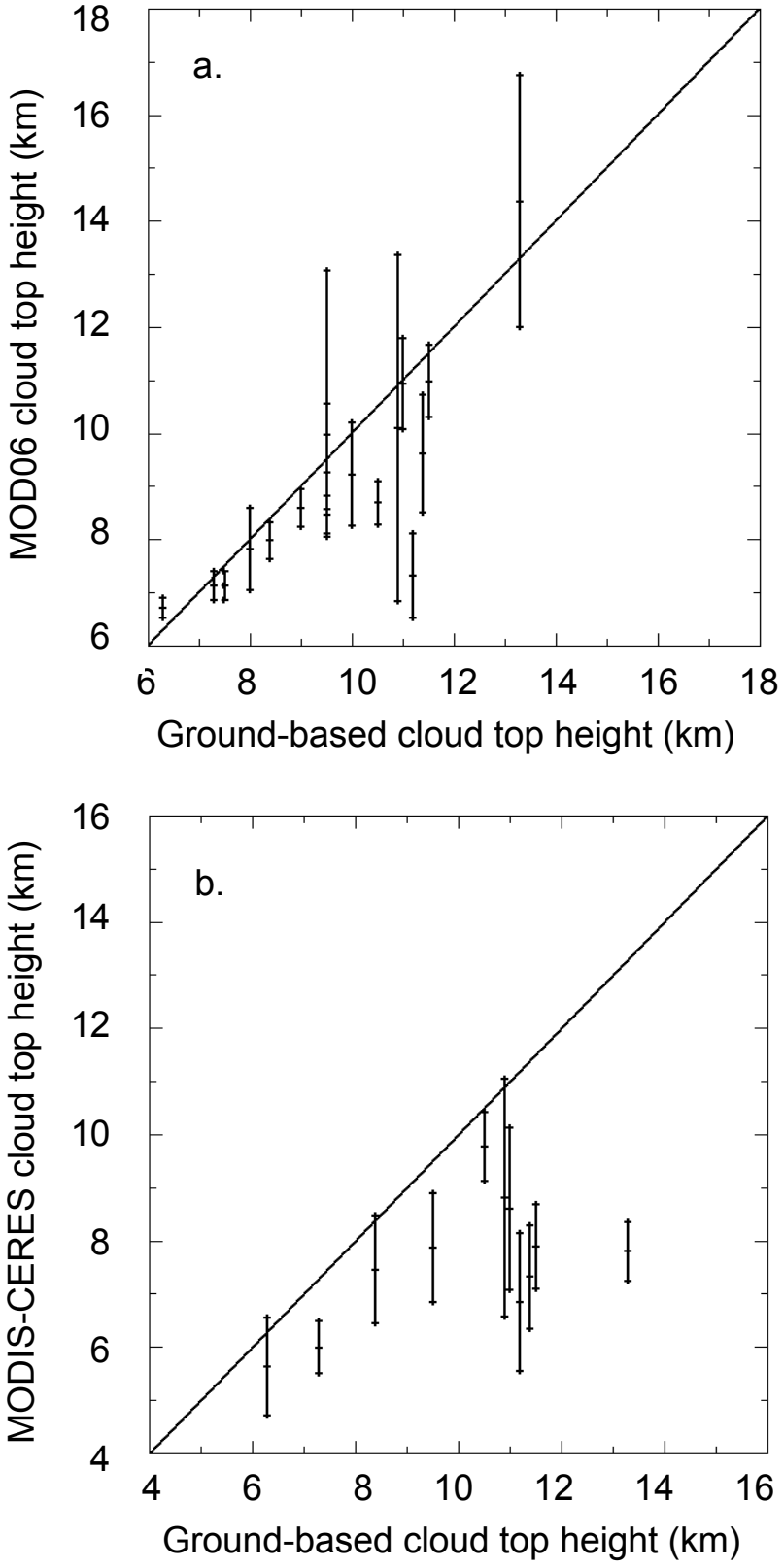

Figure 14. Comparison of cloud top heights reported by (a) the MOD06 product and (b) the MODIS-CERES products with observations at the ARM SGP site.

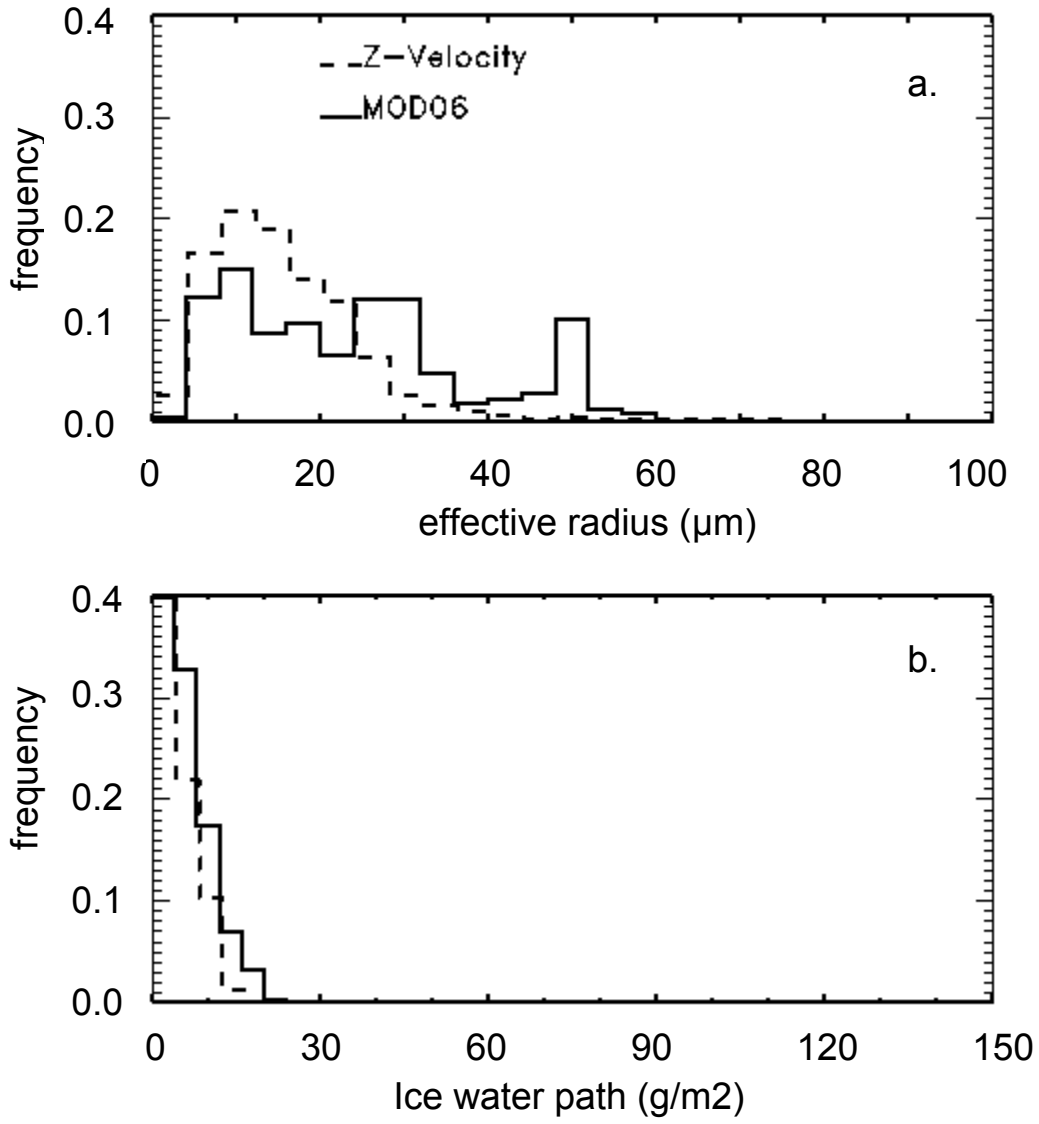

Figure 15. Comparison of the frequency distributions of effective radius (a) and ice water path (b) for cirrus with optical depths less than 0.5. The MOD06 properties are derived from a 100x100 km region centered on the ARM site for the period beginning in March 2000 and extending to July 2001. The Z-Radiance statistics are derived from cirrus clouds observed during this time period.

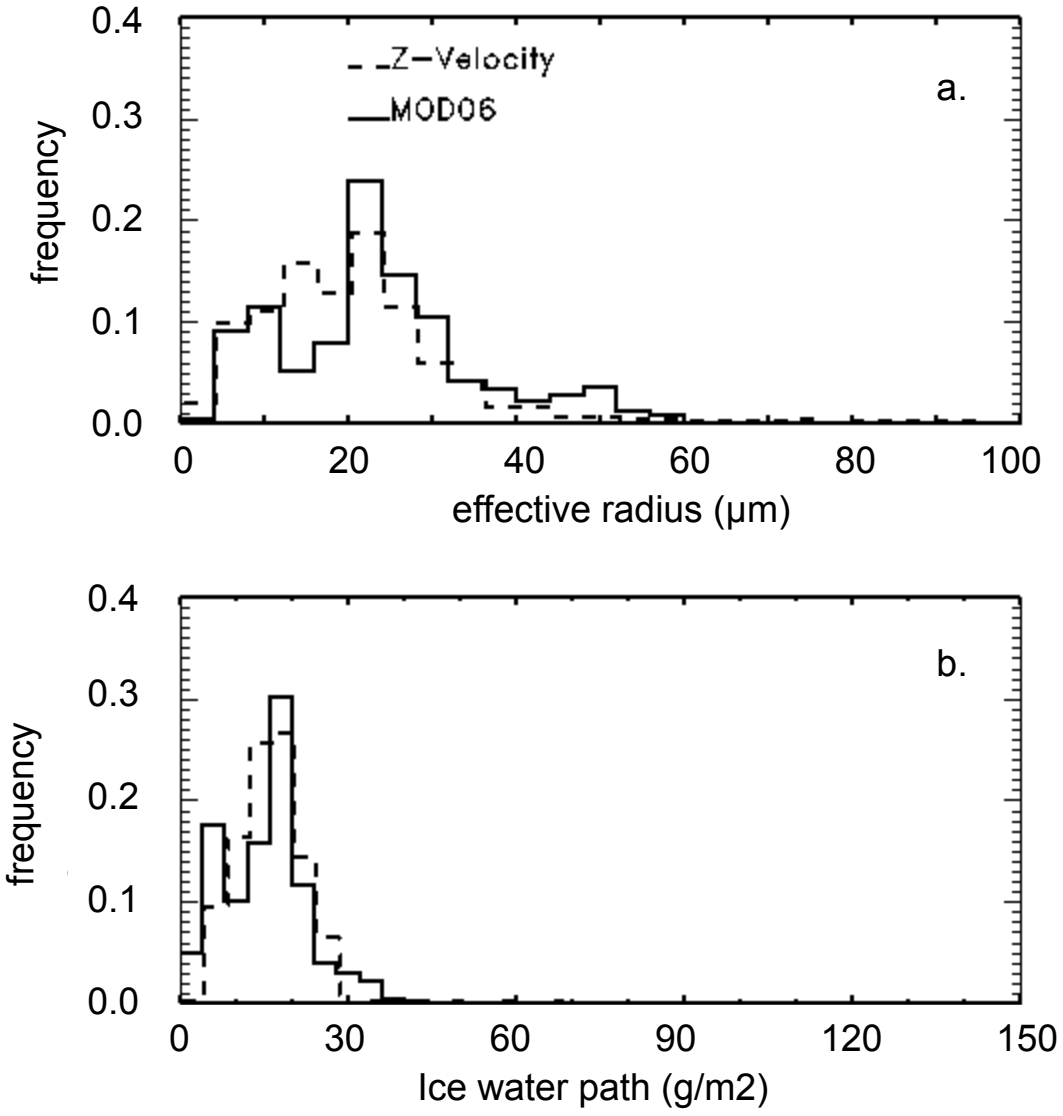

Figure 16. As in Figure 15 except for optical depths between 0.5 and 1.0

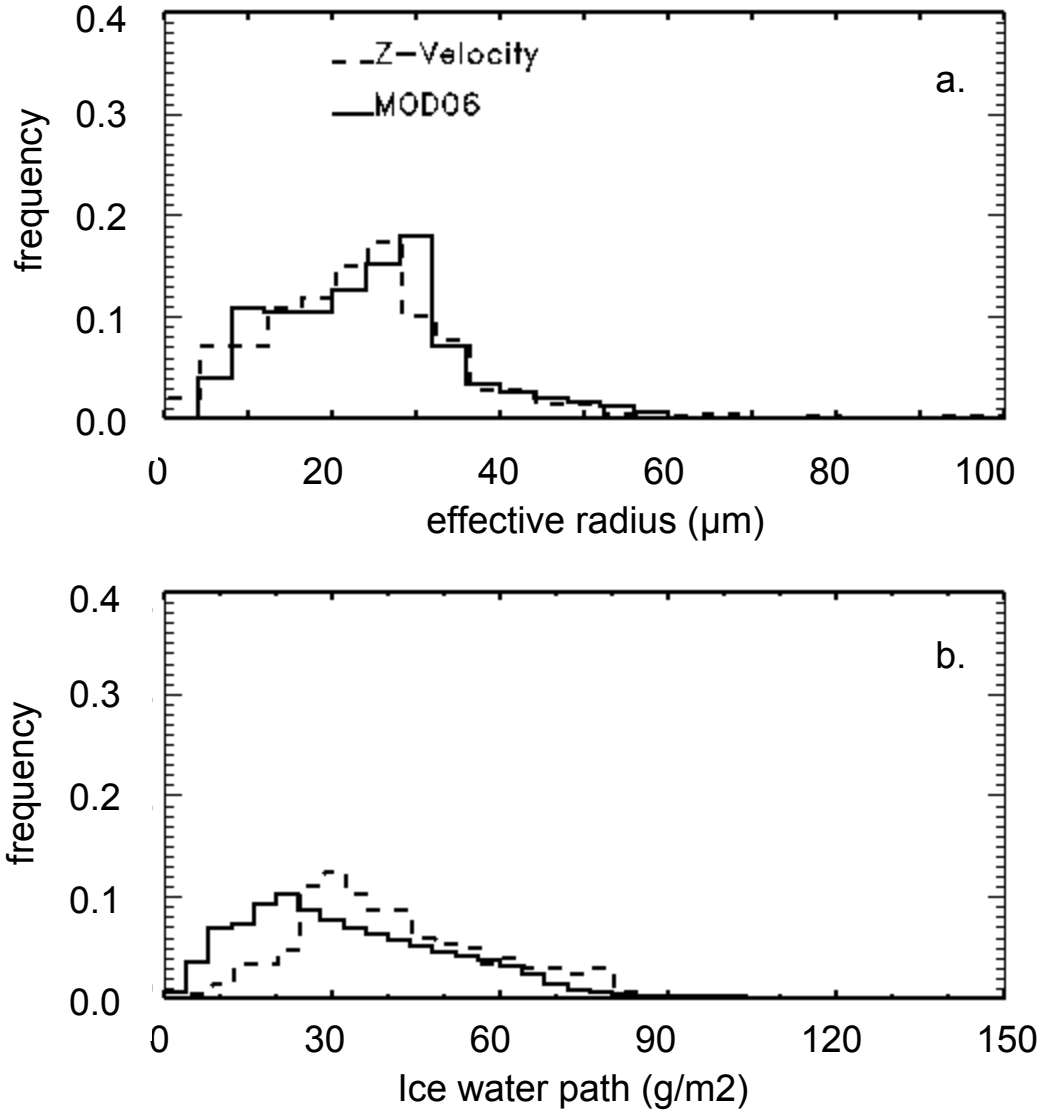

Figure 17. As in Figure 15 except for optical depths between 1.0 and 3.0

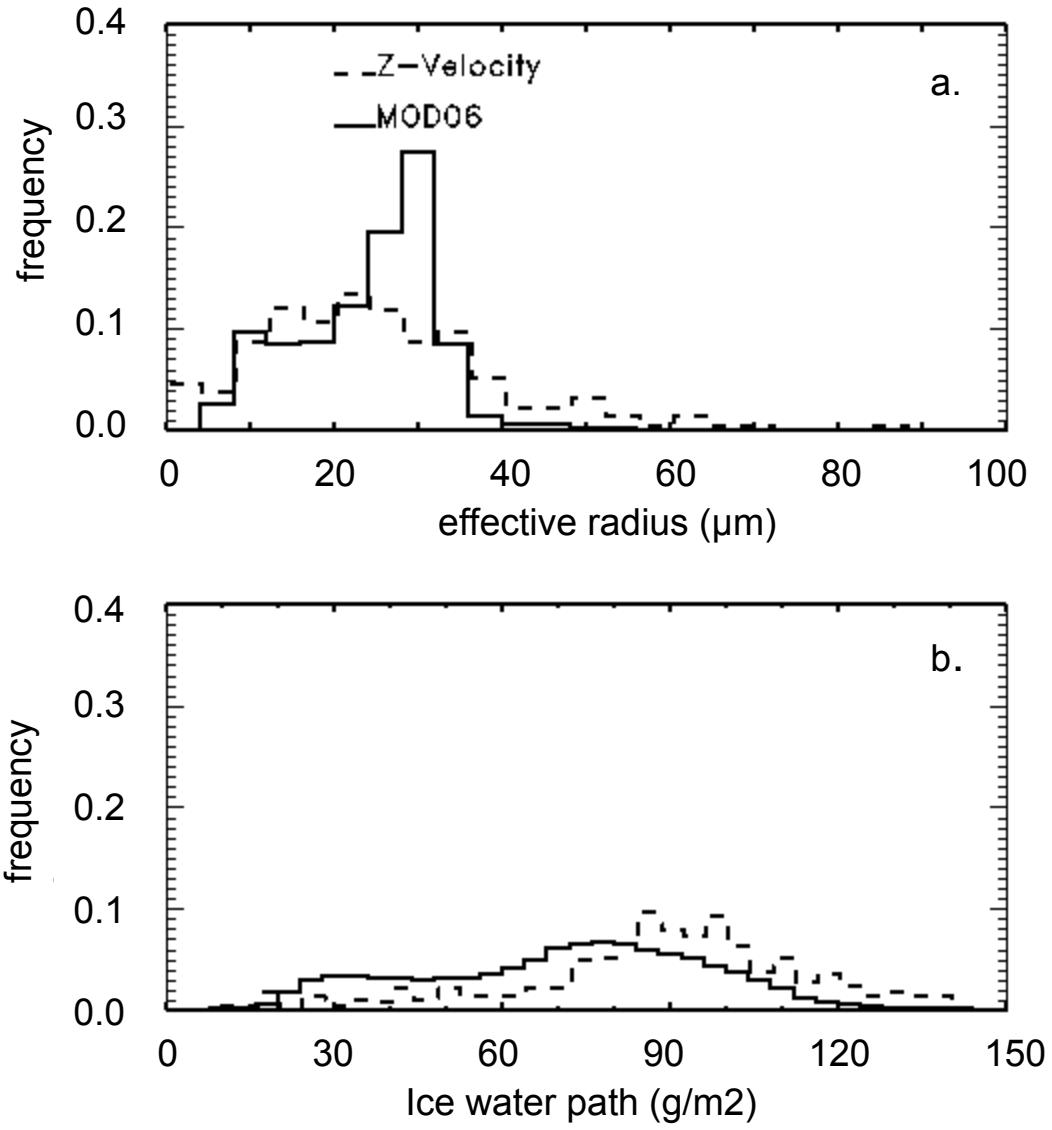

Figure 18. As in Figure 15 except for optical depths between 3.0 and 5.0

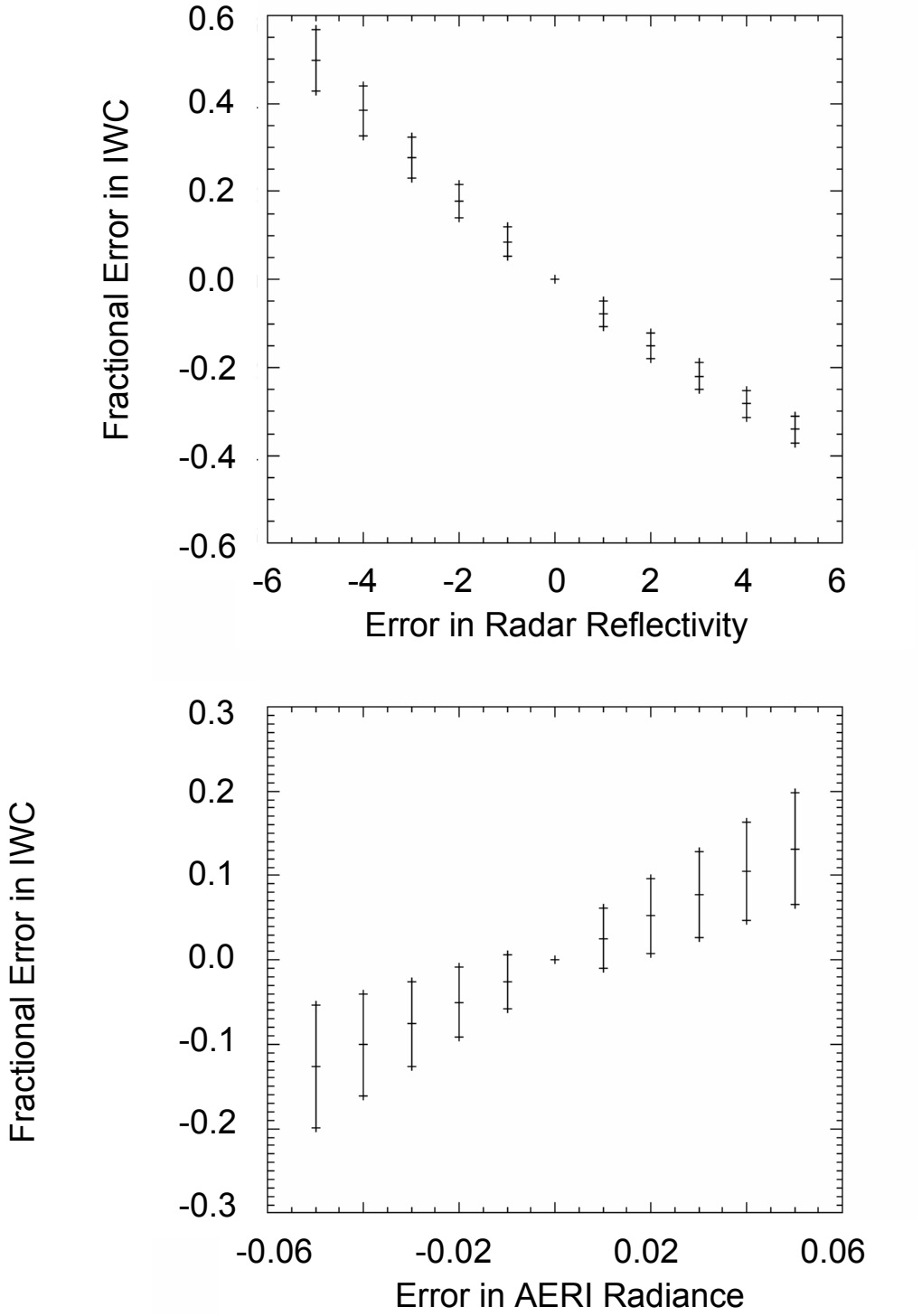

Figure A1. Sensitivity of the IWC retrieved by the Z-Radiance algorithm due to error in the input data.

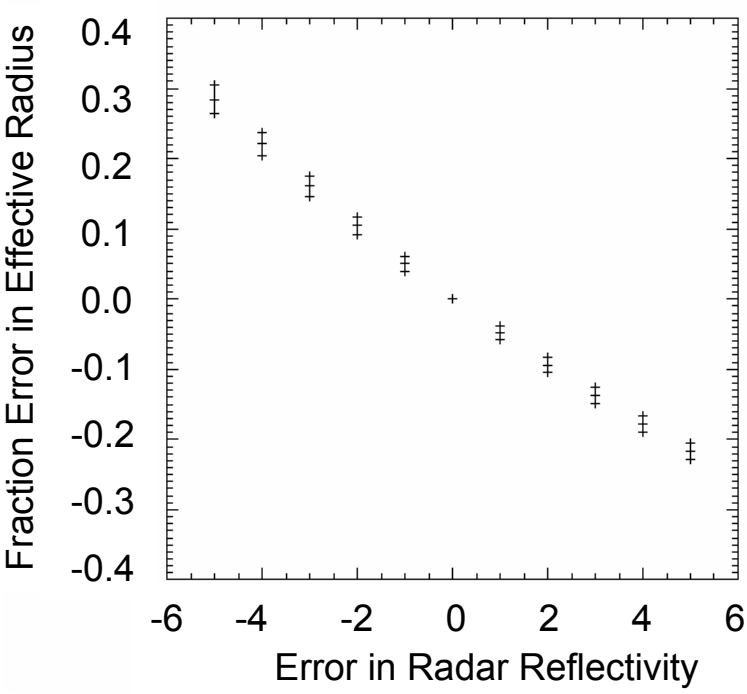

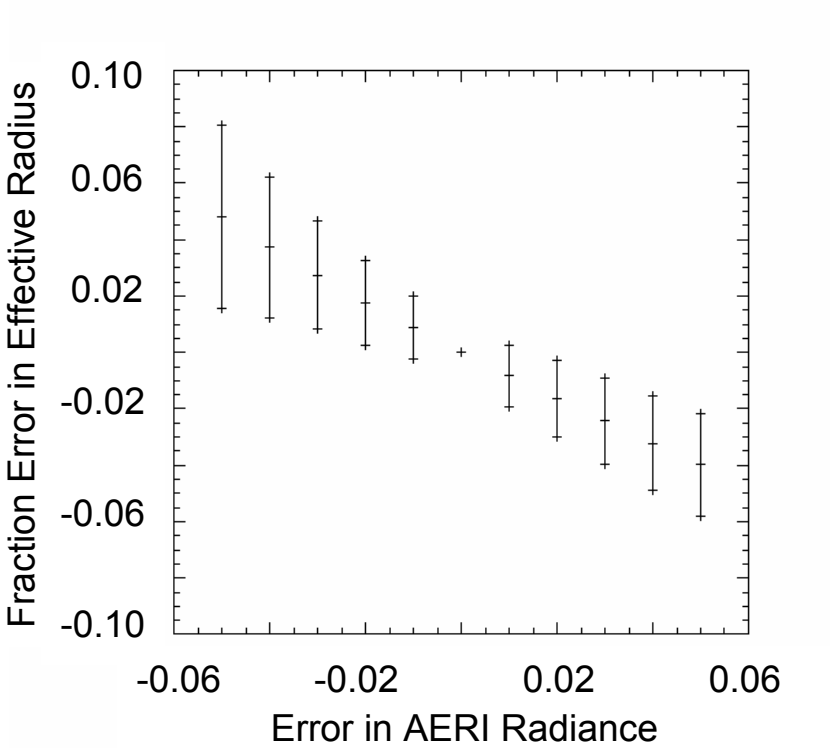

Figure A2. Sensitivity of the effective radius retrieved by the Z-Radiance algorithm due to error in the input data.

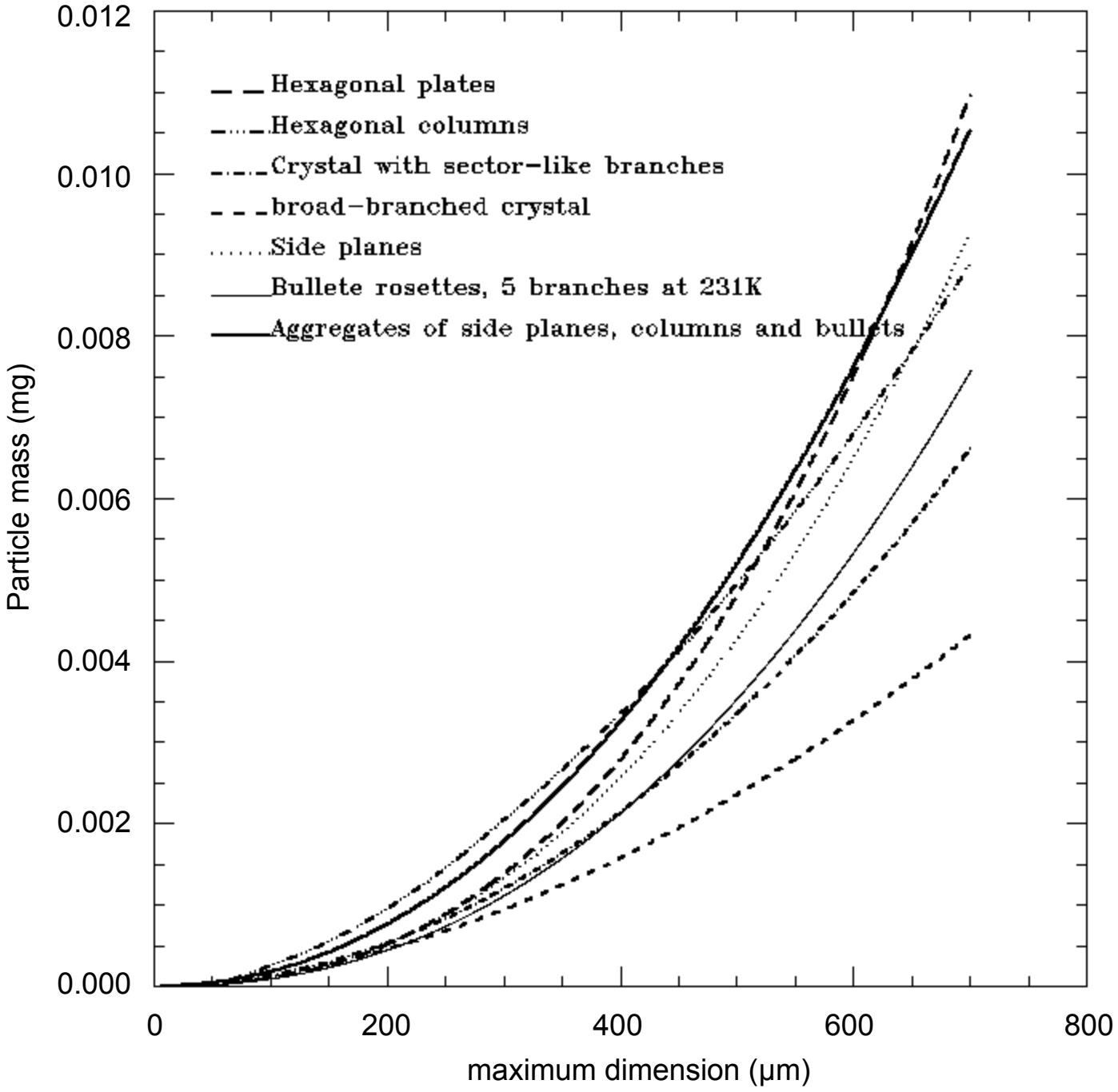

Figure A3. Mass-dimensional relationships used in the calculation of IWC from aircraft data.

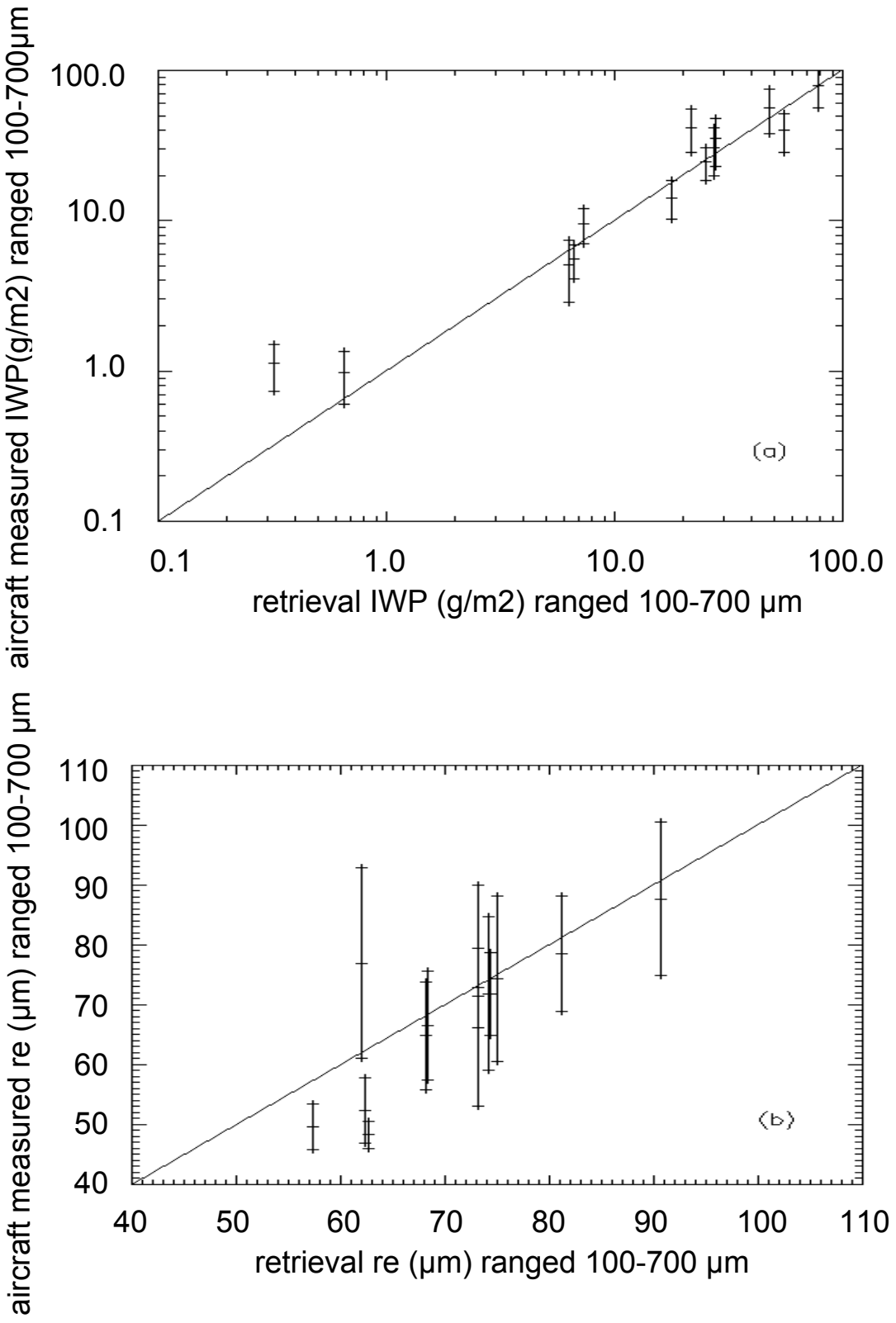

Figure A4. Comparison of aircraft-observed IWP and effective radius with retrieved values from the surface instruments. Due to limitations in the 2dc instrument, the observed and retrieved size distributions are integrated only over the 100-700 micron particle size range.

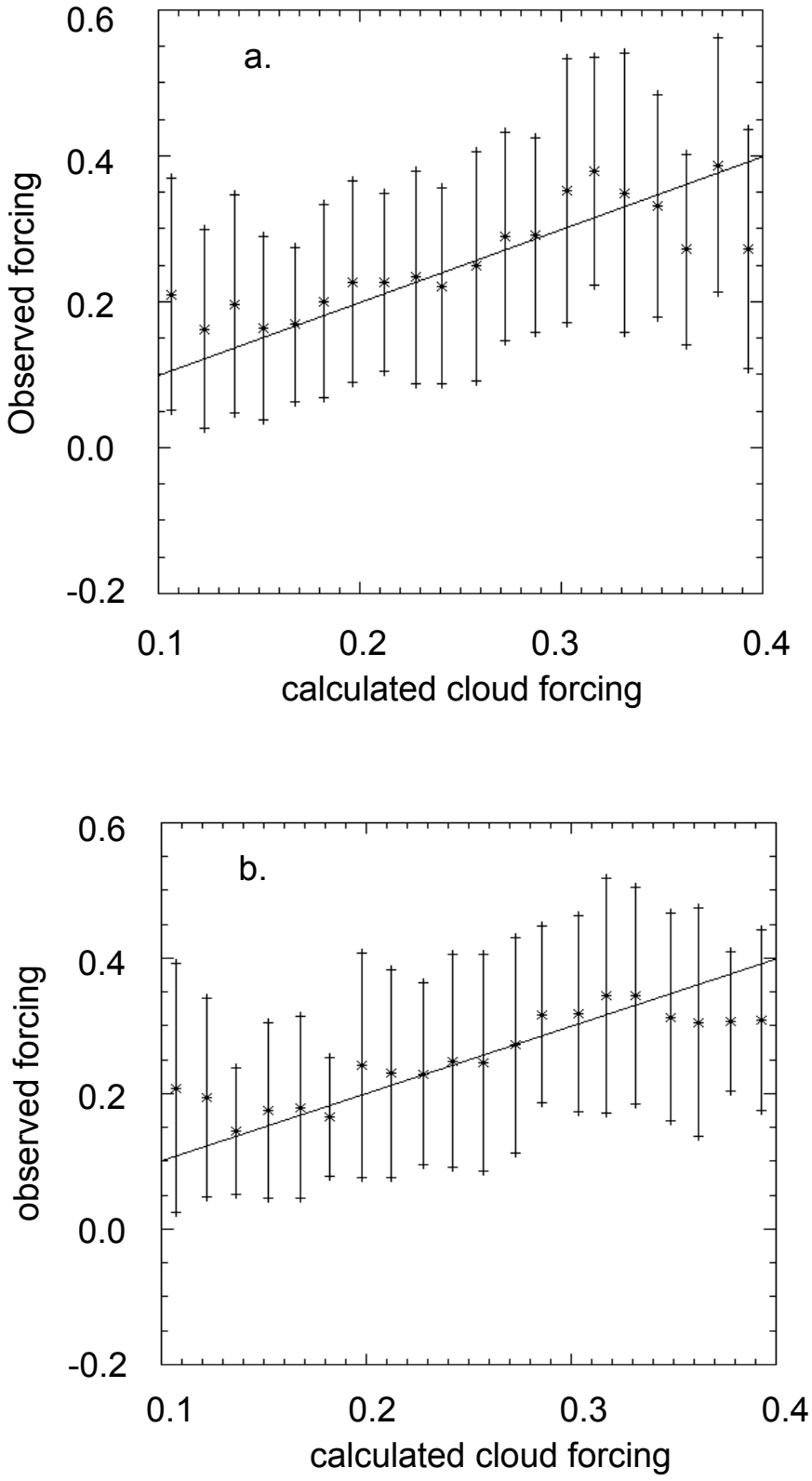

Figure A.5 Comparison between calculated and observed downwelling solar fluxes at the surface expressed in terms of the fraction of the downwelling solar flux removed by cloud. (a) solar forcing calculated from Mace98 algorithm, (b) solar forcing calculated from the improved reflectivity-radiance algorithm.

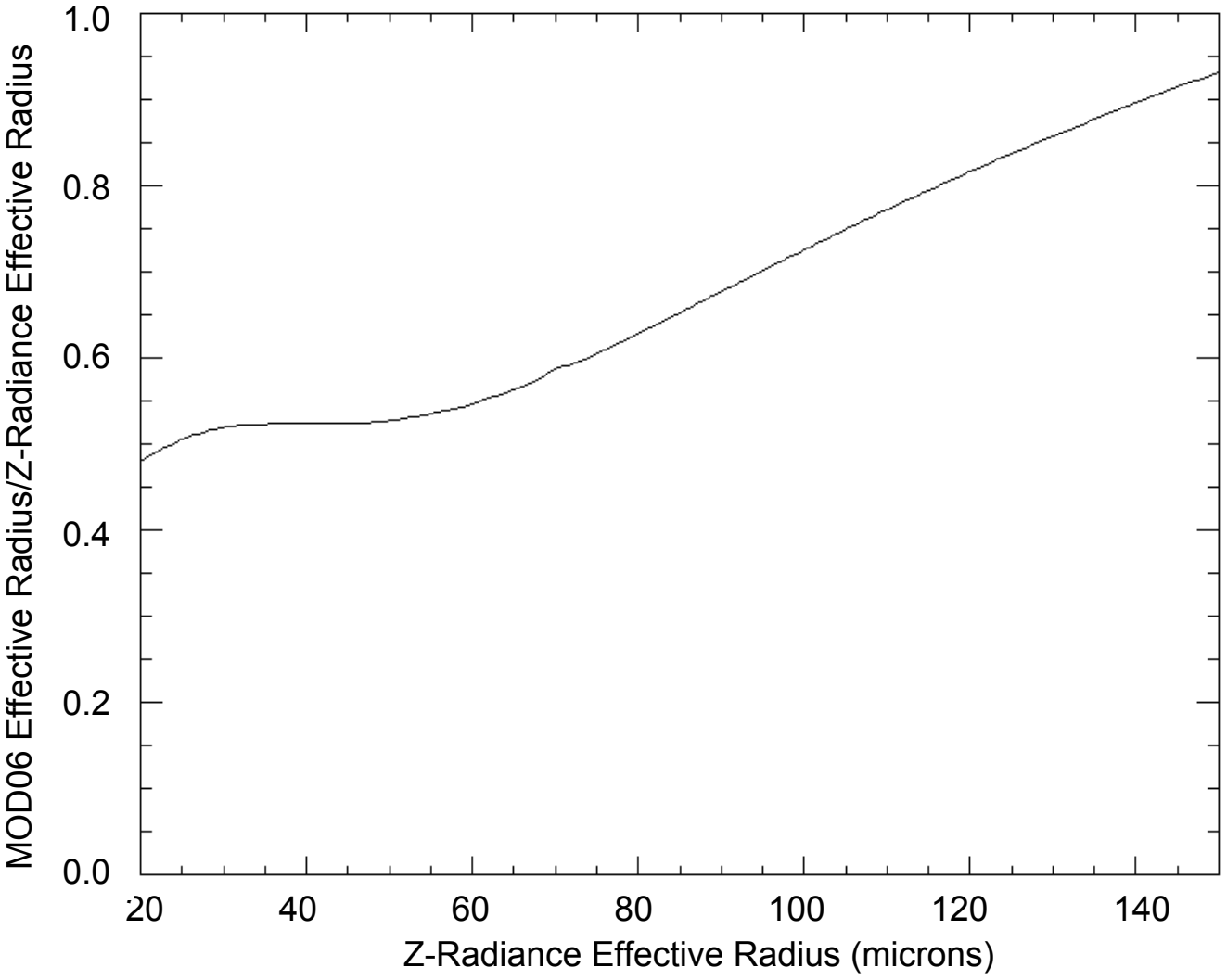

Figure B1. Ratio of the effective radius definition used in the MOD06 algorithm with that used in the Z-Radiance algorithm as a function of the Z-Radiance effective radius.